Florida International University

FIU Digital Commons

FIU Electronic Theses and Dissertations | University Graduate School

3-27-2020

Parametric Studies of Reciprocating-Flow Heat Transfer in a Reciprocating Loop Device

Majid Abdulmajeed Almas
malma016@fiu.edu

Follow this and additional works at: https://digitalcommons.fiu.edu/etd

 Part of the Mechanical Engineering Commons

Recommended Citation

Almas, Majid Abdulmajeed, "Parametric Studies of Reciprocating-Flow Heat Transfer in a Reciprocating Loop Device" (2020). *FIU Electronic Theses and Dissertations*. 4533.
https://digitalcommons.fiu.edu/etd/4533

This work is brought to you for free and open access by the University Graduate School at FIU Digital Commons. It has been accepted for inclusion in FIU Electronic Theses and Dissertations by an authorized administrator of FIU Digital Commons. For more information, please contact dcc@fiu.edu.

FLORIDA INTERNATIONAL UNIVERSITY

Miami, Florida

PARAMETRIC STUDIES OF RECIPROCATING-FLOW HEAT TRANSFER IN A RECIPROCATING LOOP DEVICE

A dissertation submitted in partial fulfillment of the

requirements for the degree of

DOCTOR OF PHILOSOPHY

in

MECHANICAL ENGINEERING

by

Majid Abdulmajeed Almas

2020

To: Dean John L. Volakis
College of Engineering and Computing

This dissertation, written by Majid Abdulmajeed Almas, and entitled Parametric Studies of Reciprocating-Flow Heat Transfer in a Reciprocating Loop Device, having been approved in respect to style and intellectual content, is referred to you for judgment.

We have read this dissertation and recommend that it be approved.

_____
Ibrahim Tansel

_____
Cheng-Xian Lin

_____
Berrin Tansel

_____
Yiding Cao, Major Professor

Date of Defense: March 27, 2020

The dissertation of Majid Abdulmajeed Almas is approved.

_____
Dean John L. Volakis
College of Engineering & Computing

_____
Andrés G. Gil
Vice President for Research and Economic Development
and Dean of the University Graduate School

Florida International University, 2020

© Copyright 2020 by Majid Abdulmajeed Almas
All rights reserved.

DEDICATION

I dedicate this thesis to my parents and friends. They have been the support and guiding beacon I needed to accomplish this.

.

ACKNOWLEDGMENTS

I wish to thank the members of my committee for their support, guidance and valuable suggestions. Here I will appreciate the time and dedication of Prof. Ibrahim Tansel from the Department of Mechanical & Materials Engineering, Prof. Cheng-Xian Lin from the Department of Mechanical & Materials Engineering and Prof. Berrin Tansel from the Department of Civil Engineering. My special thanks go to my major advisor Prof. Yiding Cao for his constant support, time and guidance. I am also grateful for the financial support of the Saudi Arabian Cultural Mission. In addition, I would like to acknowledge the financial support from my university in Saudi Arabia King Abdulaziz University. Finally, I want to extend my appreciation to all the faculty members and staff of the Department of Mechanical and Materials Engineering at Florida International University.

ABSTRACT OF THE DISSERTATION

PARAMETRIC STUDIES OF RECIPROCATING-FLOW HEAT TRANSFER IN A RECIPROCATING LOOP DEVICE

by

Majid Abdulmajeed Almas

Florida International University, 2020

Miami, Florida

Professor Yiding Cao, Major Professor

It is anticipated that clean vehicles such as Electric Vehicles (EVs) may dominate ground transportation in the future. Reliable and lower-cost batteries are essential to the growth of EV industries. A literature review reveals that if non-uniformity of battery operating temperature reaches about 9.0 ^{o}C, the capacity of the battery pack could drop by more than 30%, Also, If the operating temperature of the battery system exceeds 40 ^{o}C or is below 0 ^{o}C, the battery power could decrease dramatically and eventually to zero. However, excellent battery thermal-management systems that improve battery capacity and operational life have yet to be developed. Since the reciprocating-mechanism driven heat loop (RMDHL) systems have both the advantages of removing a large amount of heat while maintaining a rather uniform temperature, it could have great potential to become an advanced cooling system for EVs.

The primary objective of this research is to conduct numerical, experimental, and analytical studies on a bellows-type RMDHL system. Specific tasks include (1) Developing a novel numerical method to simulate the reciprocating flow in the RMDHL; (2) Design and

fabricating a suitable heat-flux evaporator to achieve a higher heat flux level; (3) Conducting extensive experiments to quantify the effects of reciprocating amplitude, frequency, and cooling water temperature on the performance of the RMDHL system; and (4) Analytically studying the power consumption and the critical displacement volume of the reciprocating driver.

The numerical results of this study indicate that the novel numerical method using a dynamic mesh technique has successfully overcome the difficulties associated with conventional methods in handling the flow boundary conditions of reciprocating flow to produce accurate and verified simulation results. They also show that the RMDHL provides superior cooling performance compared to the conventional DPDHL cooling systems. The experimental studies have produced detailed results for heat transfer rate and temperature distribution as a function of reciprocating amplitude, frequency, cooling water temperature, and power consumption. The results are summarized in a semi-empirical correlation that provides a useful design tool for the thermal engineer community. Finally, the analytical studies have verified the derived analytical results for critical displacement volume and power consumption of the driver.

TABLE OF CONTENTS

CHAPTER PAGE

LIST OF FIGURES

FIGURE PAGE

ABBREVIATIONS AND ACRONYMS

A	Area (m^2)
$\dot{Q}$	Heat generation rate ($J/cm^2.s$)
I	Current (amp)
h	Vapor latent enthalpy (J/kg)
M	Molar mass (kg/mol)
p	Pressure (Pa)
q	Heat flow (J/s)
R	Gas constant (J/mol/K)
T	Temperature (K)
t	Time (s)
$\vec{u}$	Velocity vector (m/s)
V	Volume (m^2)
V	Voltage
$\bar{V}$	Speed

Greek Letters

μ	Viscosity
ρ	Fluid density (kg/m^3)

k	Turbulence kinetic energy [J/kg]
ε	Dissipation rate [J/kg.s]
λ	Thermal conductivity [W/m.K]
α	Permittivity
η	Efficiency

Subscripts or Superscripts

cap	Capillary
hr	Hours
i	Inner
in	Inlet
min	Minimum
max	Maximum
out	Outlet
f	friction
p	piston
w	walls

1. Chapter 1: Introduction

1.1. Motivations

Efficient thermal solutions have become enabling techniques to reduce production time and costs that are two important factors of success or failure for commercial advancement of microelectronic chips [1]. To compound this problem, the trend in the manufacturing of microelectronic chips shows that there is a reduction in size while the heat flux increases for better performance. In general, the heat flux of microelectronic chips is high. An example of this would be 10 W heat generation through a 5 mm x 5 mm substrate, resulting in a heat flux as high as 400 W/cm^2 [2][3][4]. There has been a projection of heat fluxes to exceed 1,000 W/cm^2 [5]. Due to these reasons there is a need to create effective methods to remove such high heat fluxes.

High heat flux is not the only issue for electronic systems. Some systems are not subjected to high temperatures, but they are prone to failure because of temperature variations [6]. These failures are due to hot spots that occur because of the non-uniform heat flux distribution. Therefore, cooling methods that could achieve both high heat-flux cooling and temperature uniformity are preferred. Efficient thermal solutions are also critical to battery packs due to the non-uniform system temperature or heat flux distribution across the cooled surfaces [7]. For lithium-ion batteries the operating temperature will have a direct impact on battery performance, and the non-uniform temperature distribution will cause the cells to be electrically unbalanced [8]. A battery module is made up of individual cells connected in series or parallel depending on the requirements of voltage and power [8]. Each battery module is comprised of their individual monitoring, thermal control and electrical

components. These battery modules are then connected in either series or a parallel arrangement, or even a mixture of both to make up a battery pack [9]. Because of its relatively large size, high heat dissipation rates, and temperature uniformity requirements, the creation of an efficient cooling method for battery packs is challenging.

One problem that faces conventional two-phase cooling systems with a traditional pump is the cavitation phenomena. A method of avoiding this problem is to sub-cool the outlet of the condenser [10]. And in order to sub-cool the system, there would be the need to add a refrigeration system, which could make the system unrealistically complicated in order to achieve the sub-cooling requirement.

The challenges mentioned above have instigated the development of the Reciprocating-Mechanism -Driven Heat Loop (RMDHL)[11]. The RMDHL is a single or two-phase heat transfer device that has the capability of achieving high heat–flux removal as well as temperature uniformity. The configuration of an RMDHL is flexible; it could be configured to cool a computer chip of small size for high-flux cooling or to maintain a temperature uniformity for a larger system such as a battery pack. Since the invention of the RMDHL, some extensive studies have been undertaken. However, in the prior studies on RMDHL systems, the emphases were mostly placed on the high heat flux and temperature uniformity. The performance effects of some of the most important operational parameters, such as the amplitude and frequency of the reciprocating driver, as well as the power consumption of the driver, were not experimentally quantified. Also, in the prior studies certain numerical simulations were conducted, but the use of conventional numerical methods proved to be ineffective in creating reciprocating flow in the loop numerically.

Furthermore, some analytical solutions were attempted, but the results that could be experimentally verifiable were not produced. For these reasons, this study is needed to address the deficiency of prior studies and provide more effective design tools for the application of the RMDHL particularly in the battery cooling area.

1.2. Background and Theories of RMDHLs

The reciprocating-mechanism driven heat loop (RMDHL) is an effective heat transfer device conceived by [11], [12]. Figure 1 shows the concept of a RMDHL driven by a solenoid-operated driver, while Figure 2 shows the configuration of an experiment apparatus employing a solenoid-driven RMDHL. The device is made of a hollow loop that is filled with a set amount of working fluid, a solenoid-operated driver that through a piston in the reservoir produces a reciprocating motion of the working inside the loop, an evaporator section to receive heat from an external heat source, and a condenser section to dissipate the received heat. Because of the reciprocating motion, the working fluid is effectively supplied from the condenser section to the evaporator section to facilitate the heat transfer from the evaporator section to the condenser section.

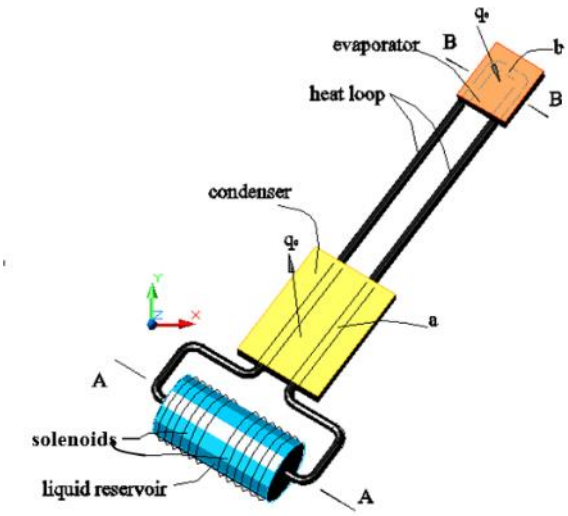

Figure 1. Schematic of a solenoid-operated RMDHL [13]

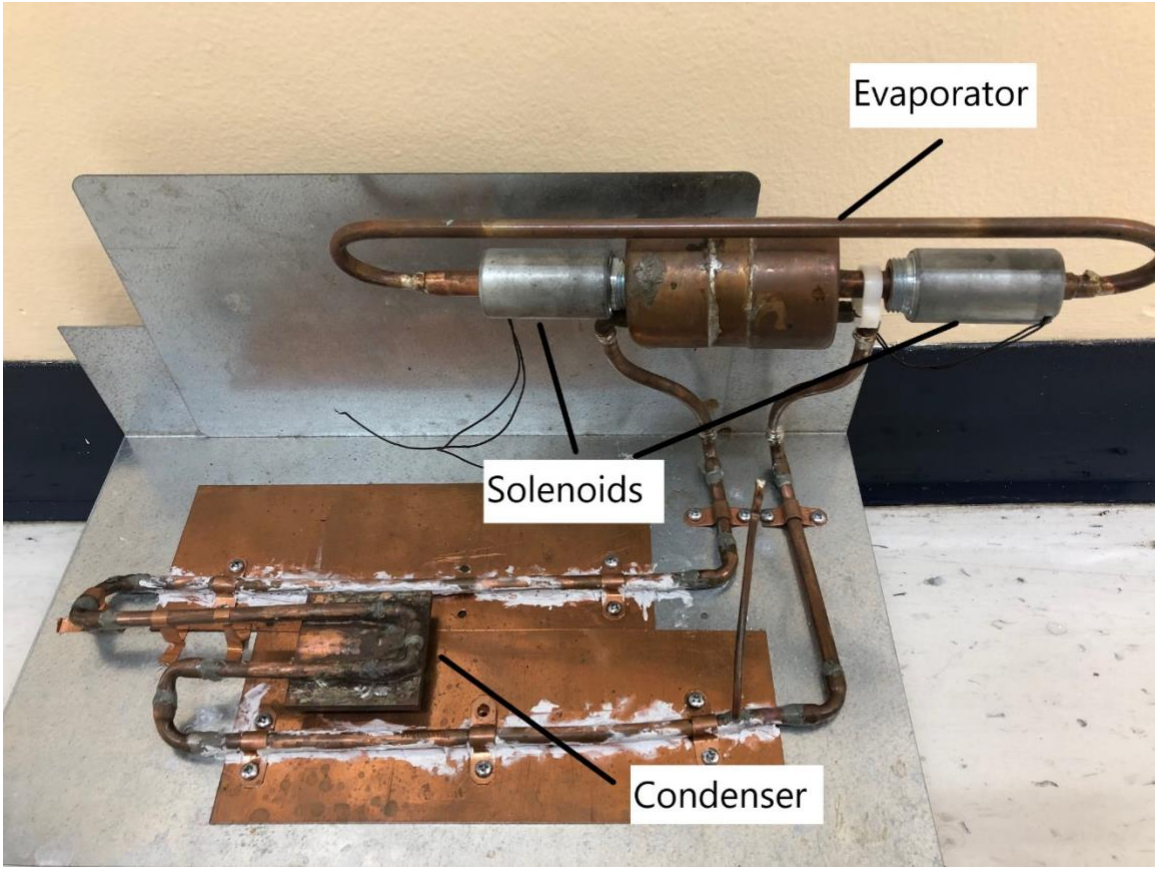

Figure 2. Configuration of a solenoid-type RMDHL for electronics cooling.

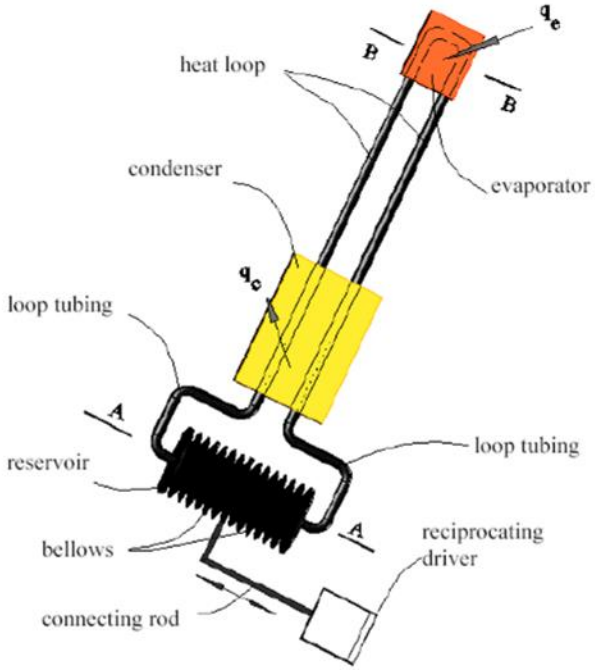

Figure 3. An RMDHL based on a bellows-type driver [11]

A unique feature of this device is that the working fluid undergoes a reciprocating motion driven by the reciprocating driver. The mixing of the working fluid in the device due to the reciprocating mechanism allows for a more uniform temperature distribution within the system. A bellows-type RMDHL was also designed by Cao and Gao [11], [12], as seen in Figure 3. The bellows are connected to a rod that undergoes a reciprocating motion to generate reciprocating motion of the working fluid under a sizable reciprocating amplitude or stroke of the driver. A benefit of such a reciprocating driven cooling system is that the heat loop does not contain any contacting surfaces in the high-temperature area so that it would work at higher temperatures. Another benefit of this design is that the exterior of the bellows can be cooled, thus adequately maintaining a lower temperature for its reliability. The experimental study conducted by [11], [12], [13] concluded that the heat loop has an effective thermal conductance of more than 120 times of copper. The experiment had a 100

W electric heater and the contact surface of the heater was 0.56 cm2 using a relatively low reciprocating frequency of 0.5 to 1.0 Hz to have achieved a stable temperature of the heated surface with minimal fluctuation.

The RMDHL works on two concepts, the first is to destroy the boundary layer developed by the flowing action of the working fluid. The fact is that the boundary layer could have a retarding effect on the heat transfer rate and the constant destruction of the boundary layer could enhance the convection heat transfer [12], [14]. Due to the motion of the reciprocating driver, the direction of the flow will constantly change. Under a sufficiently higher reciprocating frequency of the driver, the boundary layer could be destroyed before it is fully established. Thus, the average heat transfer coefficient could be increased to a level substantially higher than that of the unidirectional flow mainly because the time-averaged boundary layer would be much thinner.

There have been studies done on oscillating cooling systems, but the working fluid is mainly a gas. Some notable research works include those undertaken by [15], [16], [17]. In order for researchers to create an efficient thermal management system, investigations are needed to improve semi-empirical correlations. Most correlations for these oscillating flow systems use unidirectional flow assumptions [18]. For improved correlations, researchers used the analytical and numerical solutions of the Naiver-Stokes equations in conjunction with experimental studies.

Sert and Beskok [19] studied forced convection heat transfer of a reciprocating flow in a two-dimensional channel numerically. They studied the effect of different parameters such as penetration length as well as the Womersley and Prandtl (Pr) numbers on heat transfer characteristics of the flow. An oscillatory pressure gradient was used to impose the periodic

velocity on the boundaries. The Instantaneous and time-averaged bulk temperature and Nusselt numbers were reported which showed that the overall convective heat transfer increases with the increase of both Prandtl number and penetration length. Friction loss and transition to turbulent for an oscillatory airflow were experimentally studied by Zhao and Cheng [20]. They introduced a correlation to predict the onset of turbulence for the oscillatory flow based on the kinetic Reynolds number and amplitude of the flow. Alam et al. [21] studied the heat transfer and thermal performance of a double tube heat exchanger both numerically and experimentally.

Bouvier et al. [22] experimentally investigated the heat transfer of oscillatory flow in a circular tube. They characterized the inverse method of heat conduction and the local heat transfer. Mackley and Stonestreet [23] showed that the oscillatory flow has the considerable enhancement of heat transfer in the periodically baffled tube. They also developed a correlation for Nusselt Number from the experimental result as well as the dynamic pressure of the flow. Different parameters on the heat transfer characteristic of the flow have been studied like Penetration length, Womersley and Prandtl (Pr) numbers, etc.

Popoola et al. [24] studied the performance of an RMDHL loop numerically for a two-phase cooling system. Their study showed that the maximum velocity in the RMDHL loop occurs near the wall compared to the maximum velocity of flow at the center of pipe for a continuous cooling loop, which results in the superior performance of the RMDHL loops. Ozguc and Akdag [25] investigated the heat transfer of oscillatory flow from a surface subjected to a constant heat flux experimentally. They used a piston-cylinder mechanism to create the reciprocating flow and conducted their experiments for different values of

oscillation frequencies and amplitudes. They also proposed a correlation for the cycle-averaged Nusselt number based on the obtained results. Mahamud and Park [26] studied the application of oscillatory flow in thermal management of Li-ion batteries numerically. Their results revealed that the reciprocating flow could reduce the temperature difference in the battery cells by more than 70% and decrease the maximum temperature of the cell by 1.5 ◦C compared to the unidirectional cooling system.

1.3. Objectives

The primary objective of this research is to conduct numerical, experimental, and analytical studies on a bellows-type RMDHL system with an emphasis on addressing the deficiency of prior studies on the RMDHL devices. Specific tasks include the following:

1. Design and fabricate a suitable heat-flux evaporator to achieve a higher heat flux level in the experiment.
2. Conduct extensive experiments using the constructed bellows-type RMDHL system to generate experimental data for heat transfer rates and temperature distributions under different reciprocating amplitudes or strokes, reciprocating frequencies, cooling water temperatures, and power input to the evaporator to quantify the effects of these parameters on the performance of the bellows-type RMDHL system.
3. Develop an effective numerical method to simulate the reciprocating flow in the RMDHL using a novel dynamic mesh technique for reciprocating flow boundary conditions.

4. Verify the accuracy of the derived critical volume displacement of the reciprocating driver using the experimental data of this study as well as the data from prior studies.
5. Analytically study the power consumption of the reciprocating driver and verify the accuracy of the derived analytical solution using the experimental data of this study.
6. Generate a new correlation for the effective thermal conductance of the bellows-type RMDHL system using the experimental data of this study as well as the data from prior studies.

1.4. Outline of the Dissertation

The upcoming chapters of the dissertation are organized in the following order:

- Chapter 2 is the literature review on the topic of reciprocating cooling, whether the fluid used is air or liquid, with an emphasis on thermal management of battery packs. It will also discuss the cooling method by the use of PCM. Furthermore, it will discuss the optimum temperature range of the battery pack and the essential components of a battery pack.
- Chapter 3 will present a numerical model using a novel dynamic mesh technique for the simulation of the RMDHL and the comparison of the RMDHL with a DPDHL.
- In chapter 4, a bellows-type RMDHL is designed and constructed, and experiments are conducted for different operational parameters, such as amplitude, frequency, input power, and inlet cooling water temperature.

Analytical models will also be presented and verified by experimental data. A correlation that compiles the effects of these parameters will be generated.

- Chapter 5 will give the conclusion and findings of this dissertation. It will also suggest certain future studies.

2. Chapter 2: Literature review

2.1. Battery pack cooling

It is anticipated that clean vehicles such as Electric Vehicles (EVs) may dominate ground transportation in the near future, and reliable and lower-cost batteries are essential to EV industries. The batteries for EVs are expected to provide high power and high energy capacity, as shown in Figure 4, while being constrained in a small space and being light in weight [27]. The power battery pack is also the highest-cost component of an EV [28]. The battery pack consists of modules that are made up of cells connected in parallel as shown in Figure 5 [29]. Figure 6a -6b shows a battery assembly for a Kia Soul with 192 polymer pouch type cells. The rated capacity of the pack is 75Ah.

Thermal management in terms of temperature and temperature uniformity is one of the critical factors for the capacity and operational life of the battery in EV. Figure 7 shows the battery capacity and operational life under different thermal conditions. The temperature difference in the figure for S1 is 2.2^{o}C for the maximum range while for S3, the difference is 8.8^{o}C. The capacity of the battery pack decreases significantly as the temperature difference increases [30].

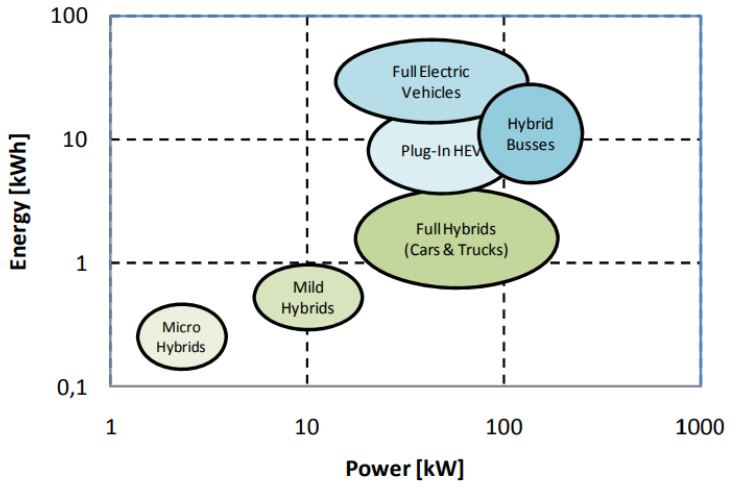

Figure 4. Energy and power ranges for battery systems in different types of vehicles [31]

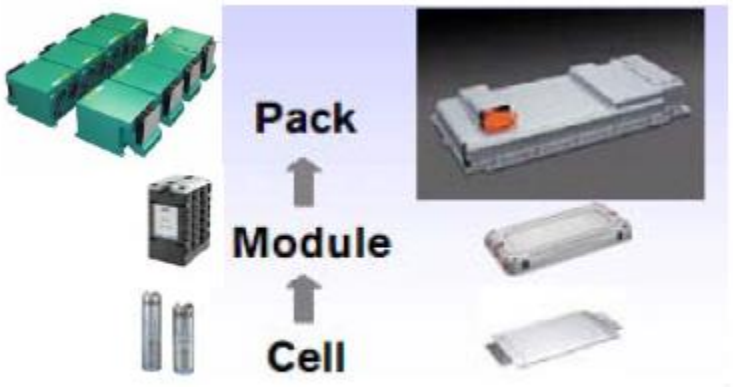

Figure 5. Cell, module, and pack [29]

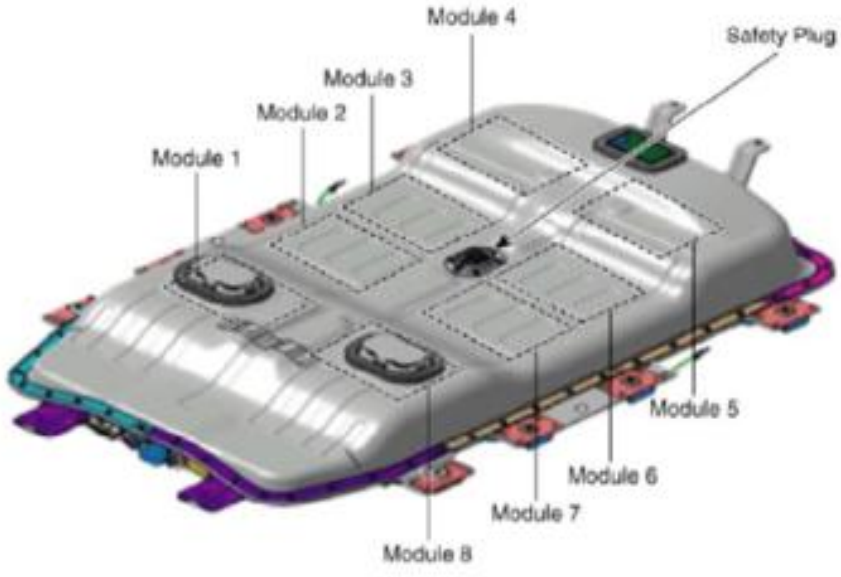

(a)

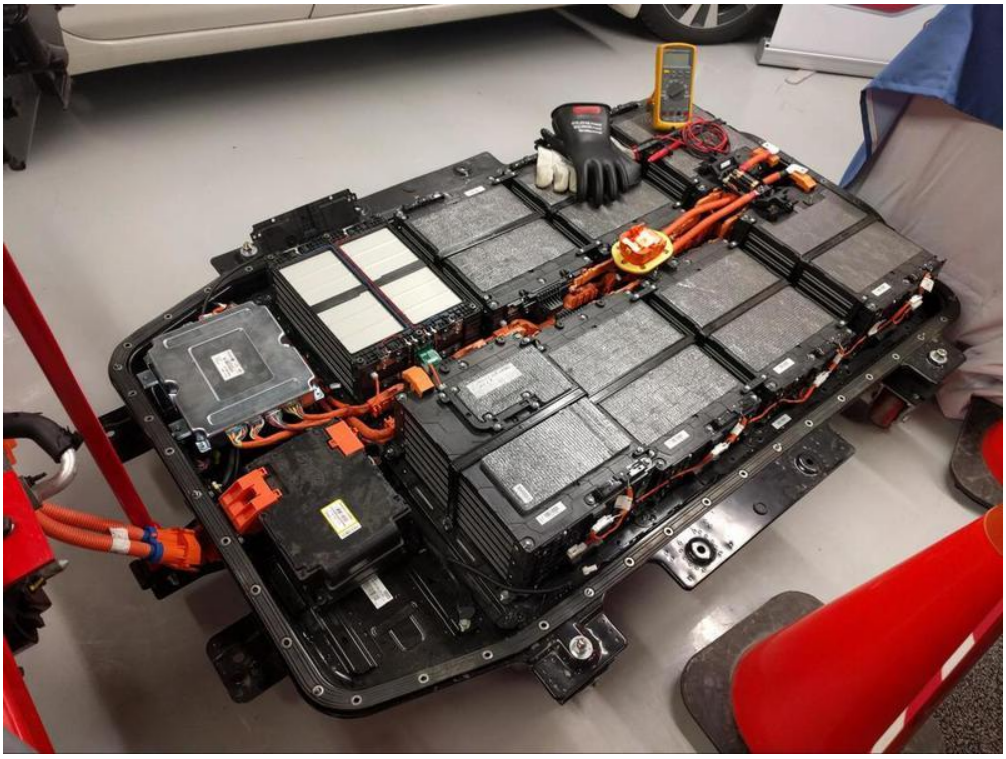

(b)

Figure 6. (a) Schematic of Kia Soul battery pack; (b) Kia Soul EV battery pack [32]

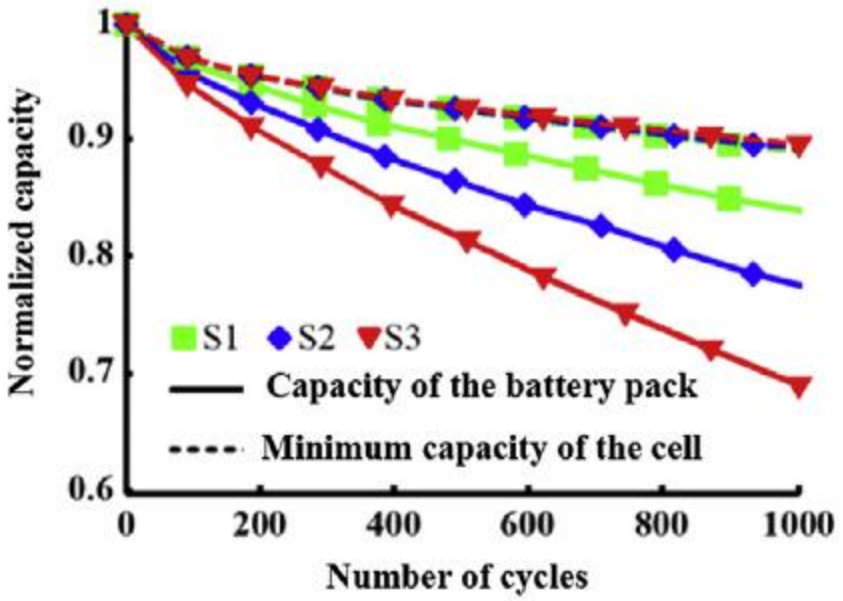

Figure 7. The capacity of a battery pack under S1, S2 and S3 [30]

The operating temperature range also has a significant effect on the performance of the battery. As shown in Figure 8 [31], for efficient operations, the operational temperature range is preferably between 20°C and 40°C. If the operating temperature is raised to above 50°C, power capability falls dramatically with the increase in temperature. On the other hand, if the operational temperature drops down to below 0 ^{o}C, the power capability would also deteriorate dramatically. If the battery cells operate in the ideal range, they could absorb waste heat, without being dissipated immediately to the cooling media. This characteristic is affected by the cell's heat capacity and other factors such as the tray of the module housing.

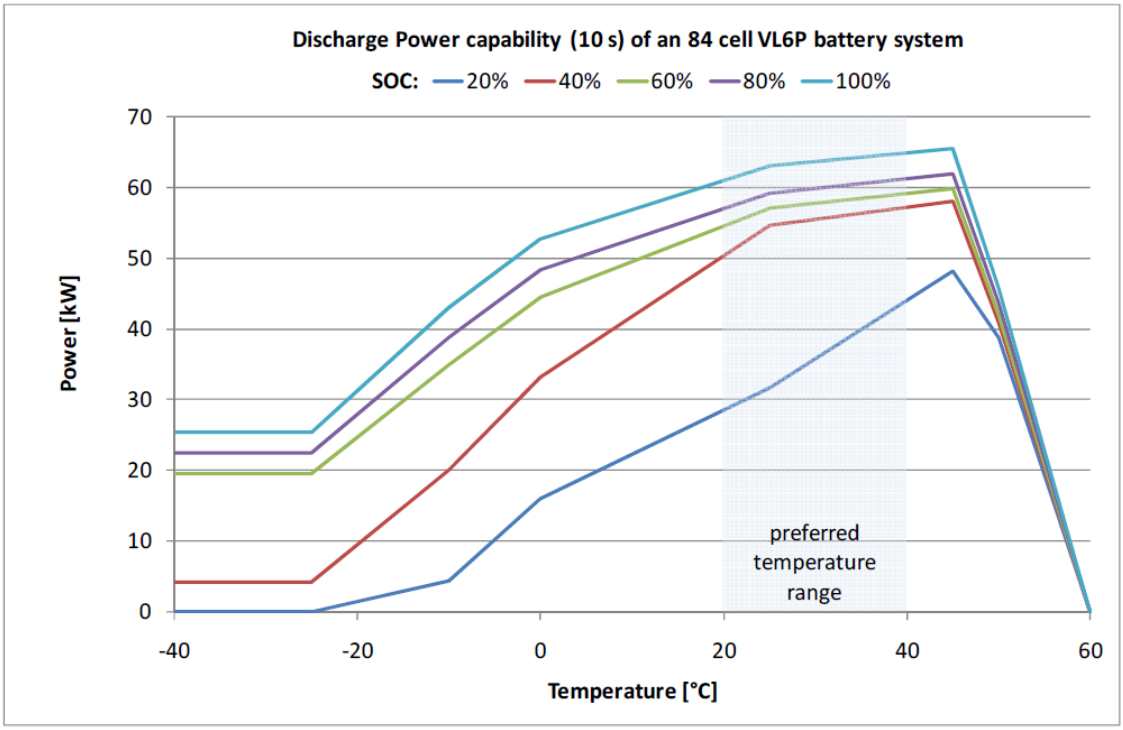

Figure 8. Discharge power capability based on temperature and state of charge [31]

The heat sources of a battery pack would be from:

1. The surroundings, such as the ambient temperature of the environment, how hot or cold the weather is.
2. The chemical reaction that is going on in the batteries.
3. Resistive losses (I^2R).

The following is a formula [33] for the heat generated in the battery:

$$\dot{Q} = I(U - V) - I\left(T\frac{dU}{dT}\right) \quad (1)$$

A huge risk in the batteries is a phenomenon known as thermal runaway. One cause of this phenomenon is the non-uniform temperature of the battery cells; therefore, in order to prevent this from happening there has to be a reliable method of cooling of these cells

[34]. Taking the li-ion life span as an example, it is reduced by approximately two months for each degree of temperature rise within its operating range of 30-40^{o}C. For optimum operating characteristics, it would be to operate below 40^{o}C and to have a temperature difference for its cell not exceeding 5^{o}C [21]. Studies show that just 5^{o}C of temperature difference would lead to approximately 10% of power capability decay, which is added to that of the long time effect of reduction of the effective operational state of charge [35]

2.2. Heat capacity

In order to design a pack or/and know how much time is needed for a pack or module to cool down, the thermal mass must be calculated. To carry out this calculation the heat capacity C_p and mass m of each component is used to get the weighted average thermal mass, given by the following formula [36]

$$m_t = \sum C_{p,i} * mi \tag{2}$$

Table 1 shows various heat capacities obtained in the National Renewable Energy Laboratory using a calorimeter shown in Figure 9. The calorimeter uses a set of heat flux sensors that measure the heat transferred (Q) between the cell and the calorimeter using the equation:

$$C_p = Q/m\ (T_m - T_c) \tag{3}$$

Table 1. Heat Capacity of selected EV and HEV Batteries [36]

Battery	**Application**	**Average Battery Temp (C)**	**Heat Capacity (J/kg/ C)**
NiMH – 20 Ah	HEV	33.2	677.4
Li Ion - 6 Ah	HEV	33.1	795
Lithium Ion Polymer – 4 Ah	EV	18	1011.8
NiMH – 90 Ah	EV	33.9	787.5
Ni MH – 6.5 Ah	HEV	32.9	521
VRLA – 16.5 Ah	HEV	32	660

Figure 9. NREL Heat Conduction Calorimeter and its test chamber [36]

In the industry, three major thermal management systems are currently in use and are divided by the cooling medium:

1. Air based cooling arrangement
2. Liquid based cooling arrangement
3. PCM-based cooling arrangement

2.2.1. Air based cooling arrangement

Although air is not the best medium to be used due to its poor properties such as low thermal conductivity, the low cost of such BTMS might be the only advantage. When the vehicle is operating in a warm environment, this system uses the air coming for the cooled passenger cabin [31]. Simply, the cells are directly cooled by airflow forced by fans. There are a number of configurations and one of them is shown in Figure 10. This configuration creates a pulsating motion by switching between the fans. When compared with the series configuration shown in Figure 11 it reduced the temperature difference from 1.3 ^{o}C to 0.6 ^{o}C, but increased the cell temperature by 0.5 ^{o}C [37].

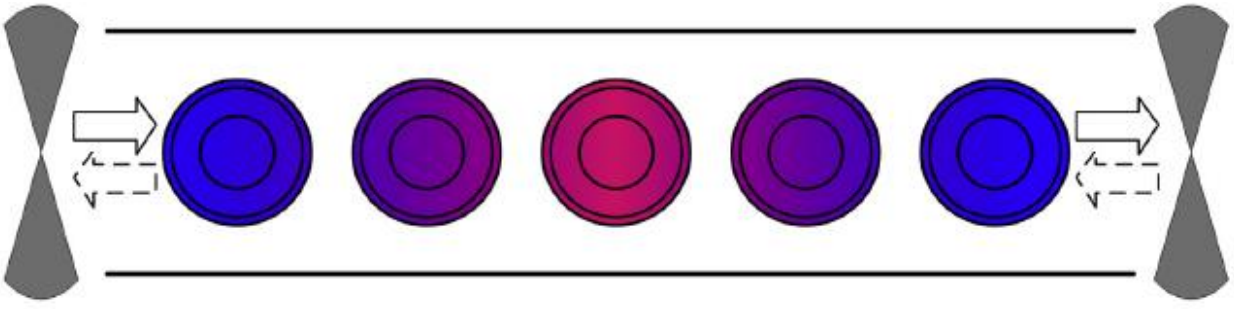

Figure 10. Simple channel with reciprocating cooling [37]

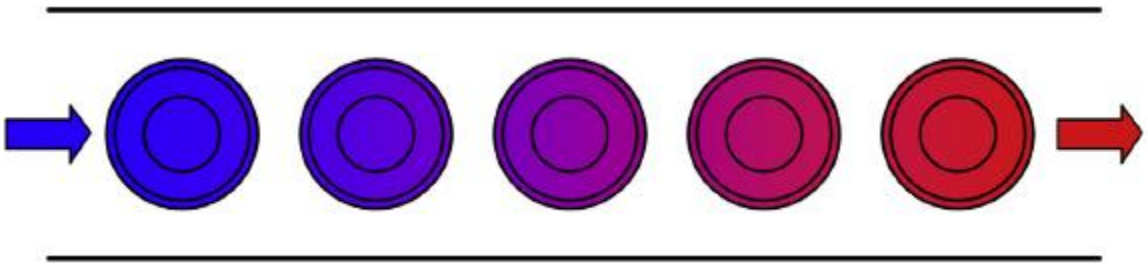

Figure 11. Series cooling [37]

An experimental study carried out by [38] as seen in Figure 12 (a) and (b) investigated the thermal behavior of an air-cooled NCM battery. The capacity of the cell is shown in Table 2 with a nominal capacity of 37 Ah and 3.65 V rated voltage.

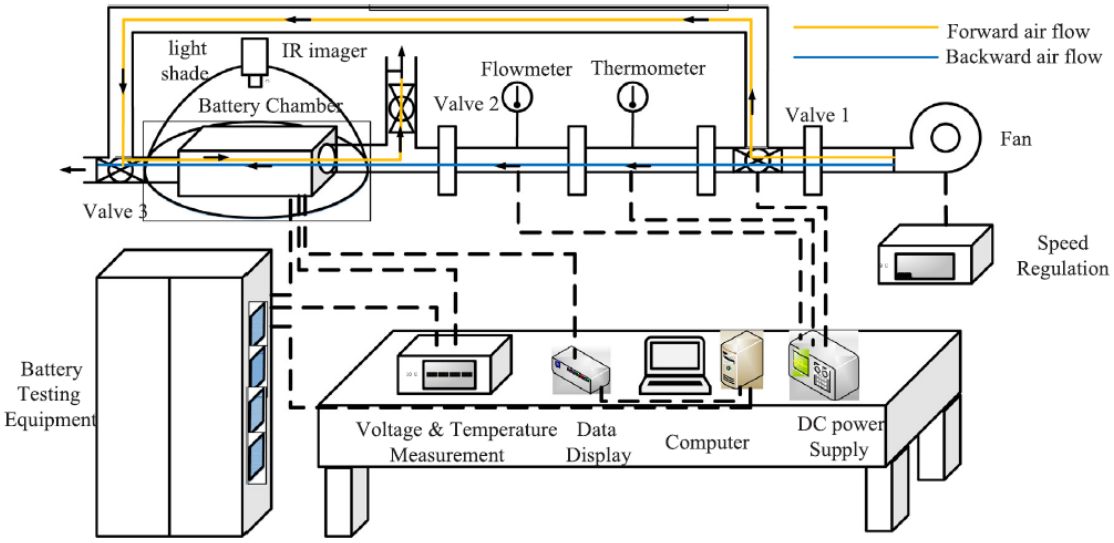

(a)

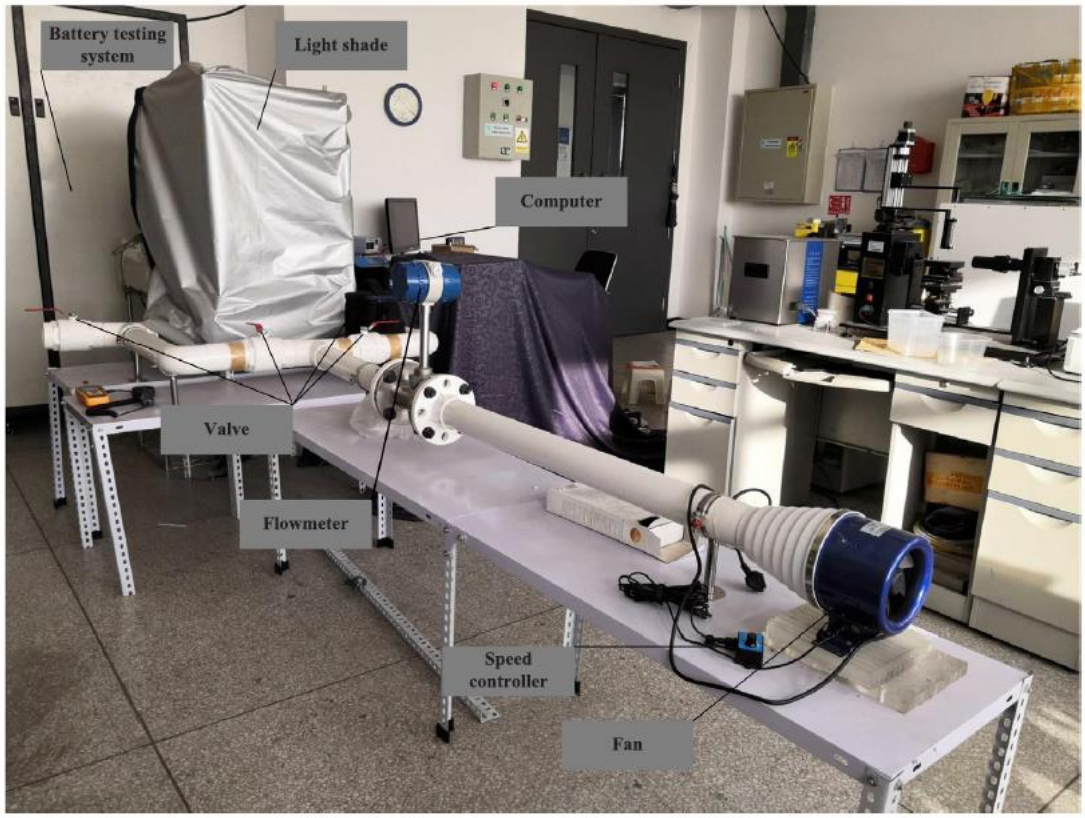

(b)

Figure 12. (a) . Schematic of the experimental system of the reciprocating air-flow (b) test rig [38]

Table 2. Battery cell parameters

Items	Parameters (mm)	Items	Parameters (mm)
Cell with (W)	211	Cell side width (W1)	8
Cell height (h)	268	Cell thickness (T)	7.1
Tab distance (A)	100	Cathode tab width (B1)	60
Anode tab width (B2)	60	Anode tab apothem (C)	25.5
Sealant height (D)	2.0	Tab height (h1)	19
Cell top sight height (h2)	19	Cell bottom side height (h3)	8

They used an infrared imager to measure the thermal distribution of the battery during forward, backward, and reciprocating air cooling flow. From the infrared images seen in Figure 13 it is clear that the reciprocating air flow provides the most uniform temperature distribution.

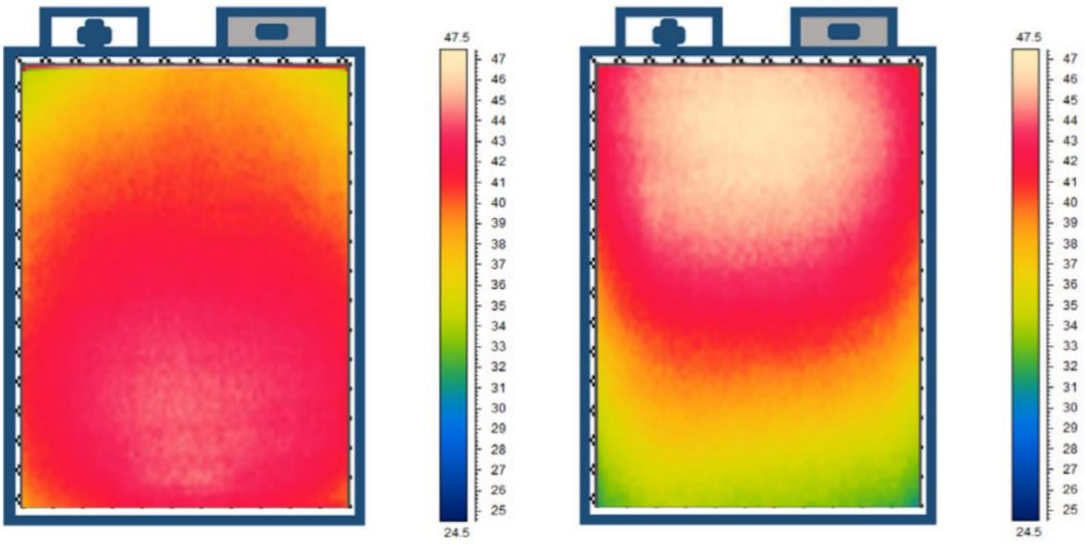

(a) (b)

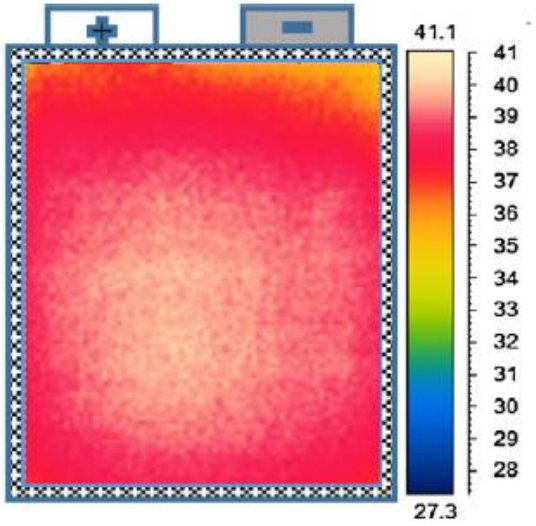

(c)

Figure 13. (a) IR image of forward air flow (b) IR image of backward air flow (c) IR image of reciprocating air flow [38]

2.2.2. Liquid-based cooling arrangement

This arrangement is more complicated than air-based cooling. For direct cooling there has to be an installation of tubing around the cells with a jacket, which either puts the cells inside a cooled or heated liquid or runs the liquid on the surface of them [35].

There are two methods of liquid cooling, direct and indirect. A system that implements direct cooling will have a high cooling capacity and be compact at the same time. A design of this unit is shown in Figure 14 where the side surfaces of the cells that don't come into contact with the heat sink plate are insulated. The difference between direct and indirect cooling is that the unit has a cooling fin in between the cells that remove or add heat to the cells by indirect cooling as shown in Figure 15 [39].

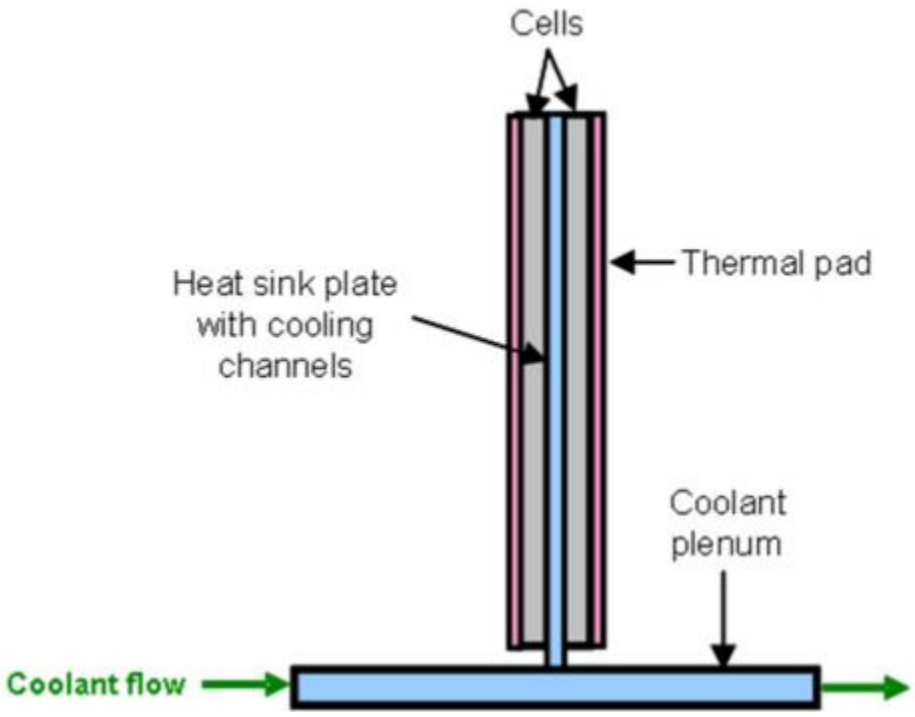

Figure 14. Illustration of a direct liquid cooling system

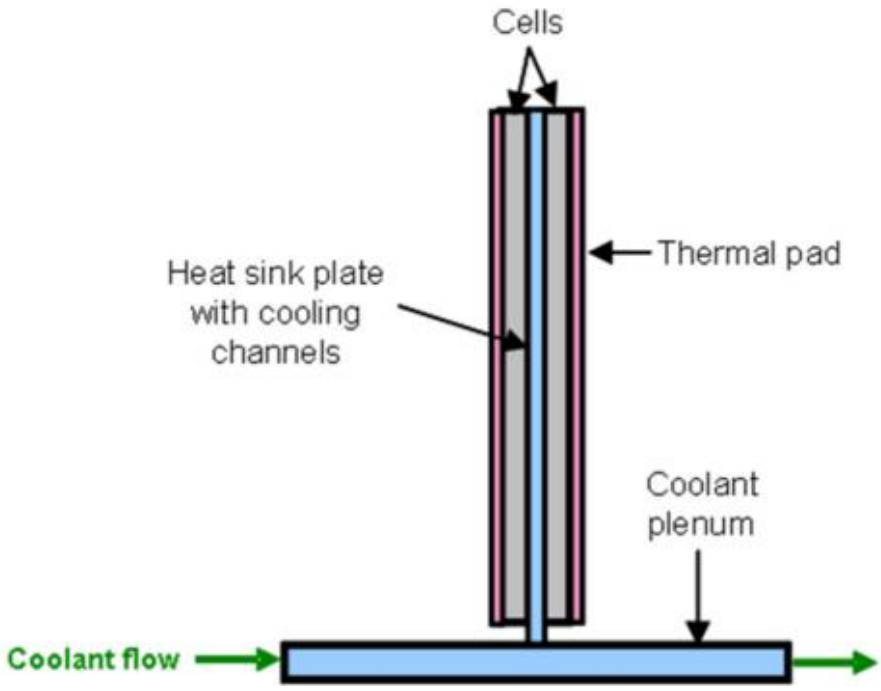

Figure 15. Illustration of an indirect liquid cooling system [39]

2.2.3. PCM-based cooling arrangement

In the battery thermal management system phase change material is used. In order to have an efficient BTMS there have to be improvements to the PCM as pure PCM has a low thermal conductivity [40]. PCMs have a large latent heat and a melting point that is satisfactory to the use in BTMS. PCM doesn't require an active cooling or heating element when the battery is operating because it causes a delay in temperature changes. In Figure 16, the gaps between the battery cells are filled with PCM and a plate that is filled with water for cooling. So, when the heat is generated from the battery it is cooled by contact with the PCM and the water cooling plate [41].

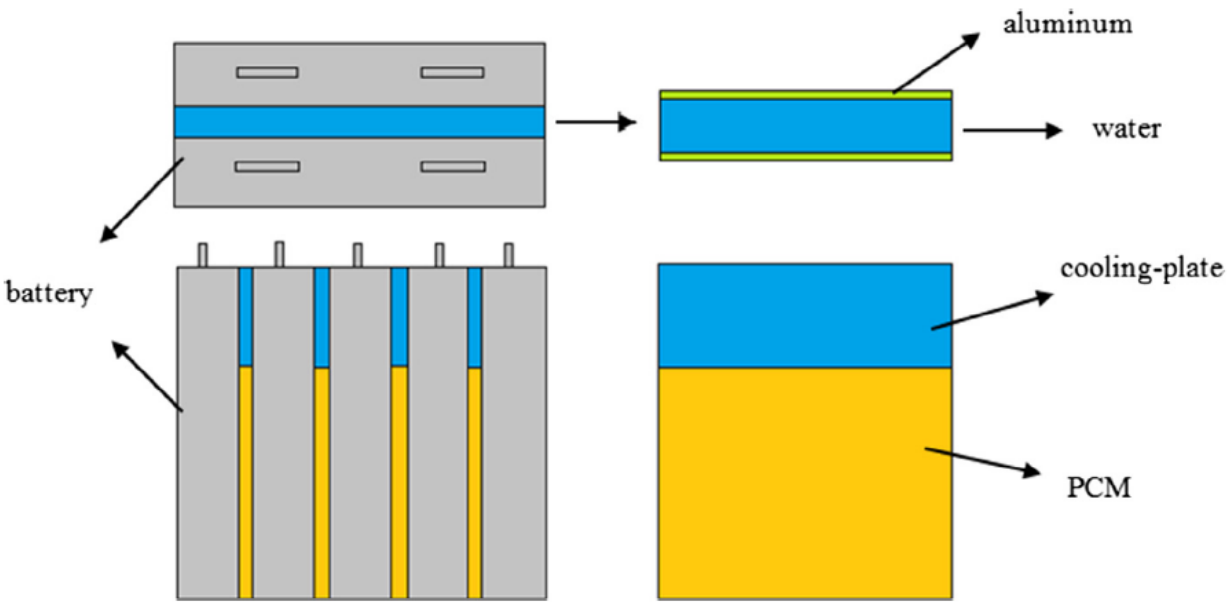

Figure 16. Schematic of lithium-ion battery module with PCM/water cooling-plate [41]

Through the above literature review, it appears that an excellent battery cooling system that improves battery capacity and operational life still does not exist. Since the RMDHL system have both the advantages of removing a large amount of heat while maintaining a rather uniform temperature, it could have a great potential to be employed for cooling battery packs of EV as a future, advanced cooling system.

3. Chapter 3: Numerical Studies

For numerical simulation of unidirectional flows, the boundary conditions at the inlet and outlet are easily prescribed. However, for reciprocating flows, special functions are needed for the specifications of the boundary conditions. These special functions may not exactly represent the conditions of the reciprocating flow created by a reciprocating driver. In this Chapter, a novel dynamic mesh method is used to generate the reciprocating flow in the cooling loop by using two moving boundaries. The numerical results are first validated by using existing relations in the literature and then the performance between an RMDHL loop and a DPDHL loop is compared.

3.1.Governing equations

The governing equations are continuity, momentum, and energy:

$$\nabla . \vec{V} = 0 \tag{4}$$

$$\rho\left(\vec{V} . \nabla V \right) = -\nabla p + \mu \nabla^2 \vec{V} \tag{5}$$

$$\rho C_p\left(\vec{V} . \nabla T \right) = k \nabla^2 T \tag{6}$$

The SIMPLE algorithm used had appropriate under-relaxation and second order discretization schemes for time and space. For the continuity momentum and energy equation the residuals were set to 10^{-4}, 10^{-6}, and 10^{-6}, respectively. In order to gauge the sufficiency of the simulation time, the average surface temperature of the heated surface was observed for the RMDHL and DPDHL loops.

The criteria for transition in turbulence in the reciprocating flow is given by [20]:

$$A_0 \sqrt{\mathrm{Re_w}} < 761 \tag{7}$$

The kinematic Reynolds number for the reciprocating flow is given by:

$$\mathrm{Re}_{\omega} = (\omega D_h^2)/v \quad (8)$$

Where v is the kinematic viscosity of the cooling liquid, ω is the oscillatory frequency, and D_h is the hydraulic diameter. The study showed that Re_{ω} for all cases was less than what was introduced by (5)

3.2. Problem Description

Figure 17 a-c shows the geometry, boundary conditions, and the computational grids for the RMDHL and DPDHL loops. The geometry consists of a circular inlet tube with 0.7899 cm (3/8 inches) diameter, rectangular channel with respective width and height of 0.2 cm and 2.4505 cm, a surface heat flux Q = 50, 000 W/m2 was mounted on the top of the rectangular channel and has the dimension of 15 cm × 2.4505 cm, six small tubes, as a cold surface, with constant surface temperature 300 K and diameter of 0.32258 cm (3/16 inches) and an outlet tube with the same dimension of the inlet tube. During this study, the temperature of the cold surface is kept constant to focus on the overall performance of the RMDHL loop, but for various applications, the cold surface can transfer the absorbed heat to the environment using forced or natural convection through the air or liquid cooling process. Extended surfaces/fins can also be used to increase the heat transfer of the cold surface in the cooling system. To model the RMDHL two in-phase moving boundaries with the same axial velocity was used. The velocity profile on both moving surfaces was defined as follows:

$$x = \frac{x_{\max}}{2}(1 - \cos \omega t) = A_0 (1 - \cos_{\omega t}) \rightarrow u$$

$$= u_{max}(\sin \omega t) \quad (9)$$

where *x*and *x*max are the instantaneous and maximum boundary displacement, A_0 is the oscillatory amplitude, ω is the frequency of the reciprocating flow, *u*and *u*max are the instantaneous and maximum velocities:

$$u_{\max} = \frac{x_{\max}\omega}{2} \quad (10)$$

The program used for this simulation is Ansys Fluent. The velocity profile is applied to the moving boundaries using the dynamic layering mesh and User Defined Functions (UDF). The continuous flow and heat transfer in the DPDHL loop was model using UDF by calculating the bulk temperature at the outlet boundary of the loop and applying the obtained temperature at the inlet of the loop until achieving the converged solution. The averaged mass flow rate in the RMDHL was set as the inlet boundary condition of the DPDHL loop hence both loops have the same mass flow rate of the water during the same period. The average mass flow rate of the cooling water was changed from 0.0152 to 0.061 kg/s in this study.

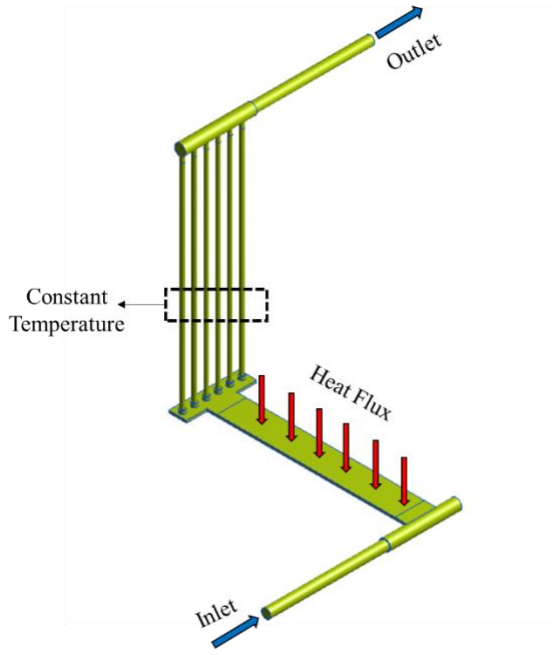
Outlet
Constant
Temperature
Heat Flux
Inlet

(a)

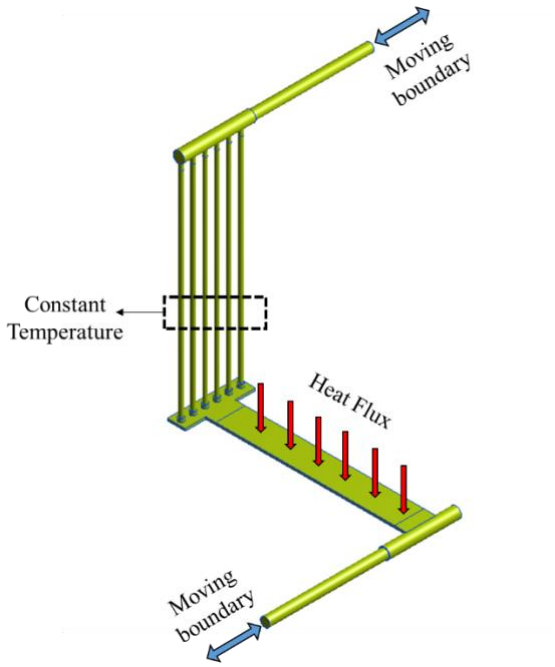
Moving
boundary
Constant
Temperature
Heat Flux
Moving
boundary

(b)

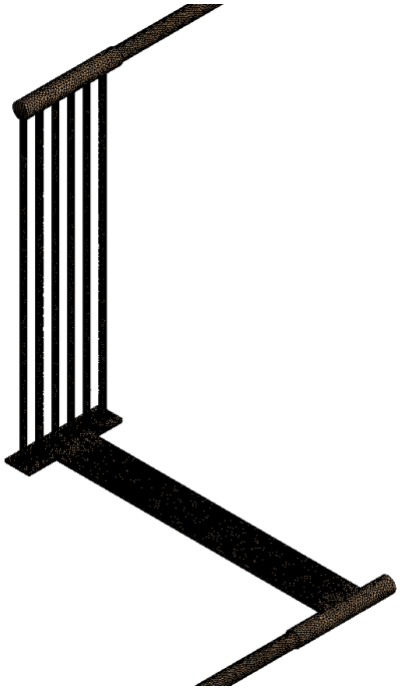

(c)

Figure 17. Schematic and boundary conditions of the (a) DPDHL loop (b) RMDHL loop and (c) and the computational grids.

Grid independence study was carried out for gird sizes 500K, 700K, and 900K, and a total control volume 700K was selected as the grid independence results.

3.3. Model validation

To validate the numerical setup for the RMDHL loop the current numerical setup is validated with the Hausen's correlation [42] for the average Nusselt number in the entry region:

$$\overline{Nu}_D = 3.66 + \frac{0.0668\left(D/L\right)\mathrm{Re}_D\,\mathrm{Pr}}{1+0.04\left[\left(D/L\right)\mathrm{Re}_D\,\mathrm{Pr}\right]^{2/3}} \tag{11}$$

The validation was carried out for a constant surface temperature circular pipe with a square wave velocity profile of the moving boundaries. The square wave velocity of the boundaries generated a constant velocity inside the circular pipe corresponding to the $\mathrm{Re}_D = 500$. Figure 18(a) and (b) show the comparison between the present simulations results and the correlation for the local and average Nusselt numbers. As can be seen, the results are in excellent agreement with the correlation.

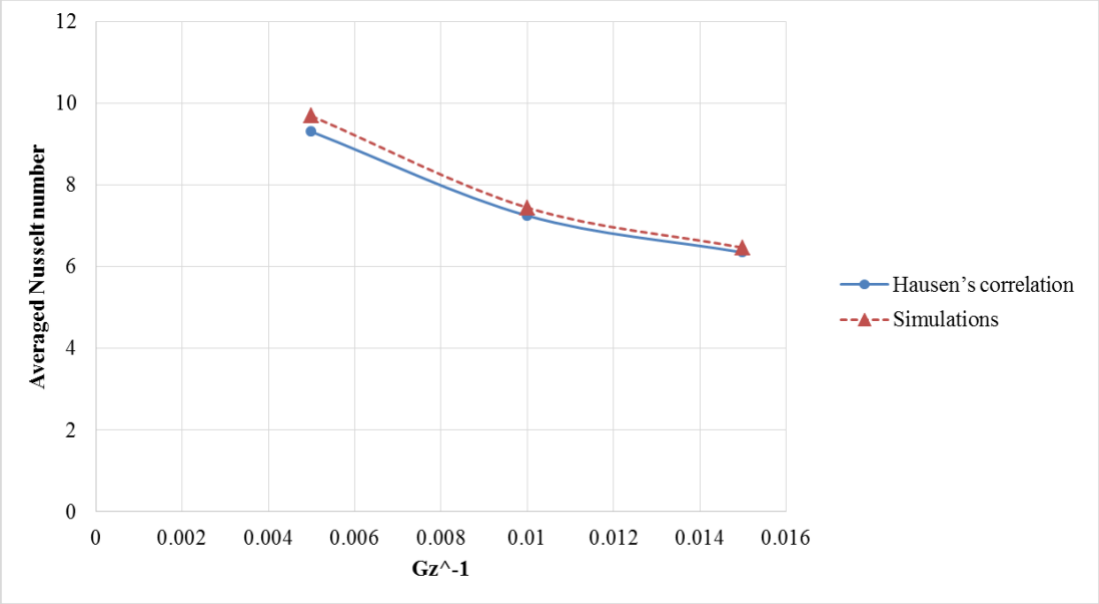

(a)

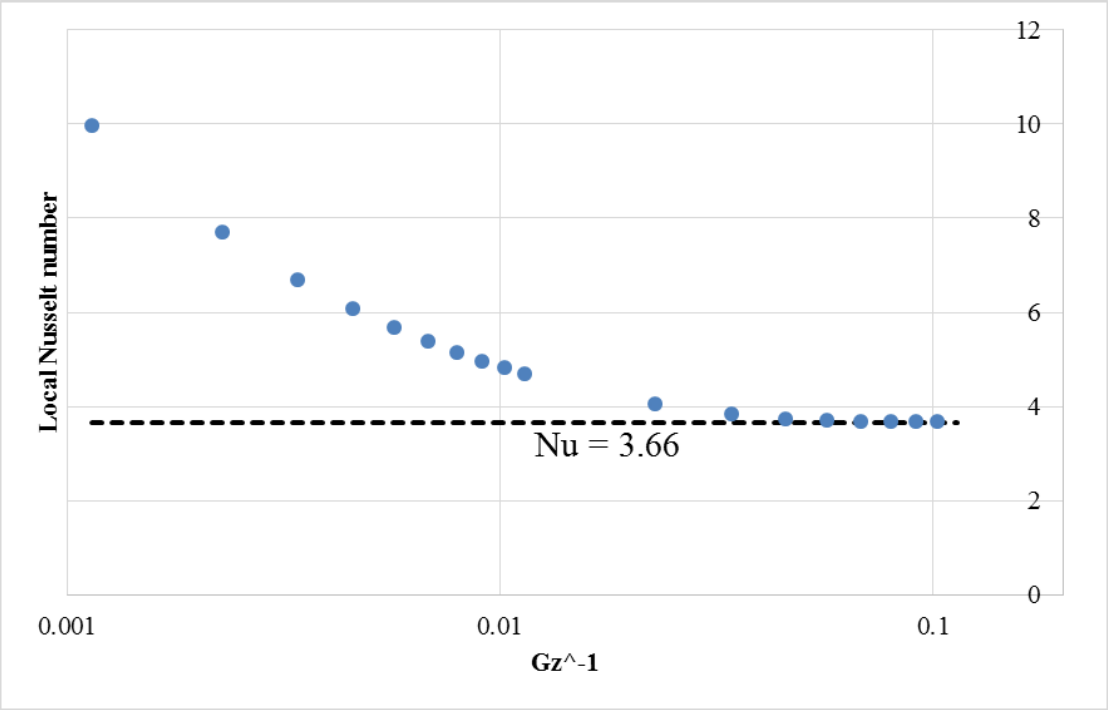

(b)

Figure 18. Validation of average and local Nusselt numbers for the RMDHL loop with a square wave velocity profile

3.4. Effect of oscillatory frequency:

Figure 19 shows the comparison between the average surface temperatures on the heated surface for the RMDHL and DPDHL loops. As seen, for the same average mass flow rate in the cooling loops the average surface temperature in the RMDHL loop is considerably lower that DPDHL for oscillatory frequencies higher than 5 Hz. Continuous change of the flow driven by the reciprocating driving mechanism in the RMDHL loops generates strong vortexes perpendicular to the flow direction which disturb the boundary layer near both heated and cooled surfaces. Moreover, these vortexes provide better mixing of the core cold/hot fluid and hot/cold fluid near the walls. For a low oscillatory frequency, the resident time for fluid in the cold /hot section of loop increases. As a result, the temperature

difference between the core fluid and the surface decrease and consequently the heat transfer rate reduces considerably.

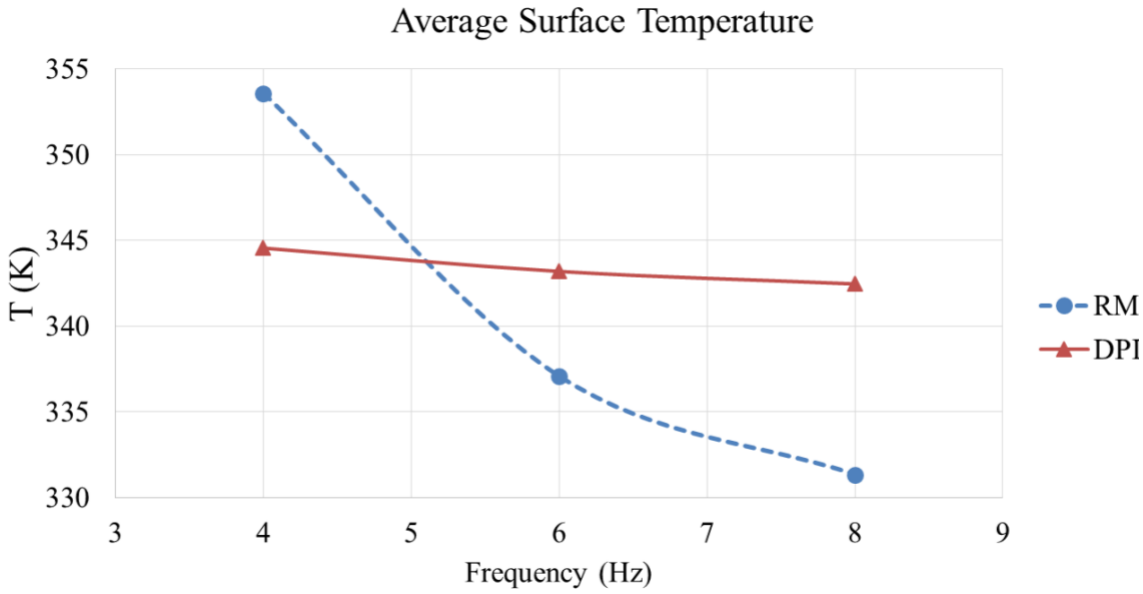

Figure 19. Effect of oscillatory frequency on the surface temperature of the heat source

Figure 20 compares the surface temperature distribution between the RMDHL and DPDHL loops. As can be seen the RMDHL loop results in a more uniform surface temperature which would reduce the thermal stress on the heated surface. Uniform surface temperature is specifically critical since a large temperature gradient on the surface of PCBs or electronic equipment, and the resultant thermal stress increases the possibility of the mechanical failure in the system. Most of the cooling methods except the ones including the phase-change process are not able to provide a uniform surface temperature. As shown in figure 5, for the RMDHL loop, the surface temperature increases greatly at the end of the heated surface due to the growth of the thermal boundary layer. The figure also shows that for the same amplitude increase of the frequency leads to a more uniform surface temperature for the RMDHL loop.

RMDHL

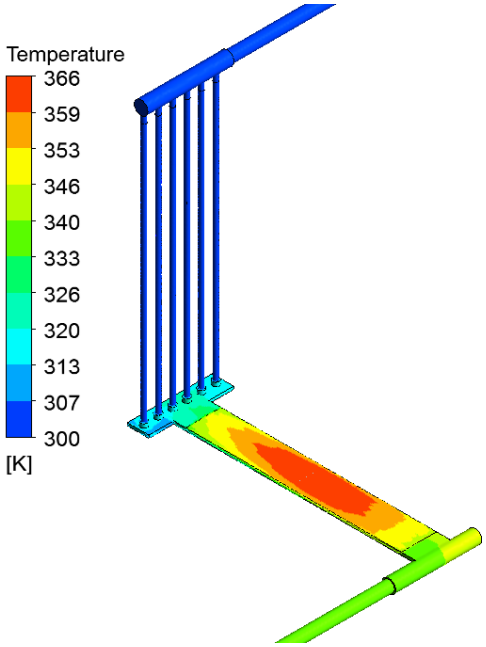

DPDHL

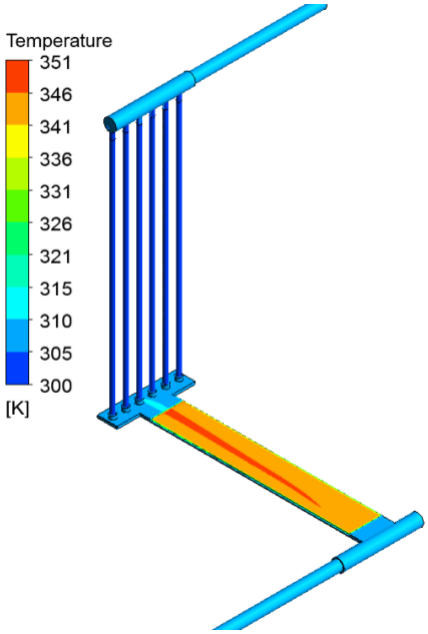

$A_0 = 0.08(m),\ \ f = 4(Hz)$

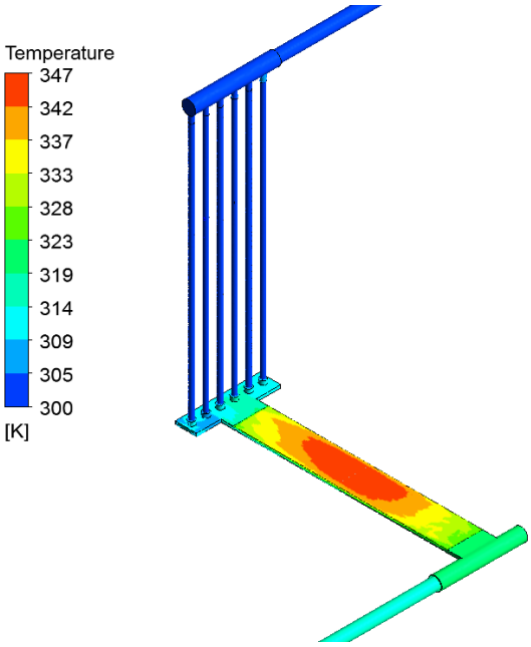

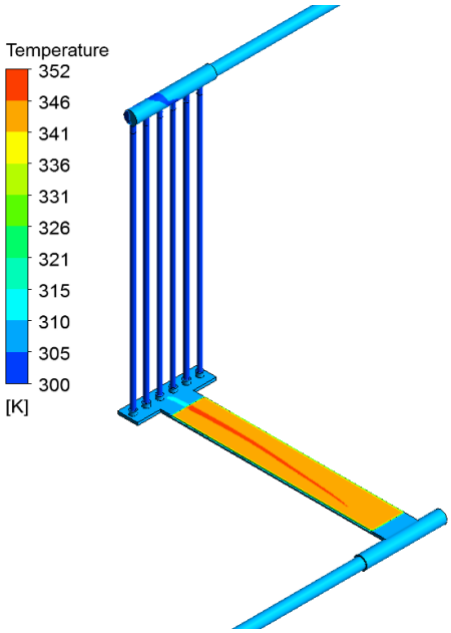

$A_0 = 0.08(m),\ f = 6(Hz)$

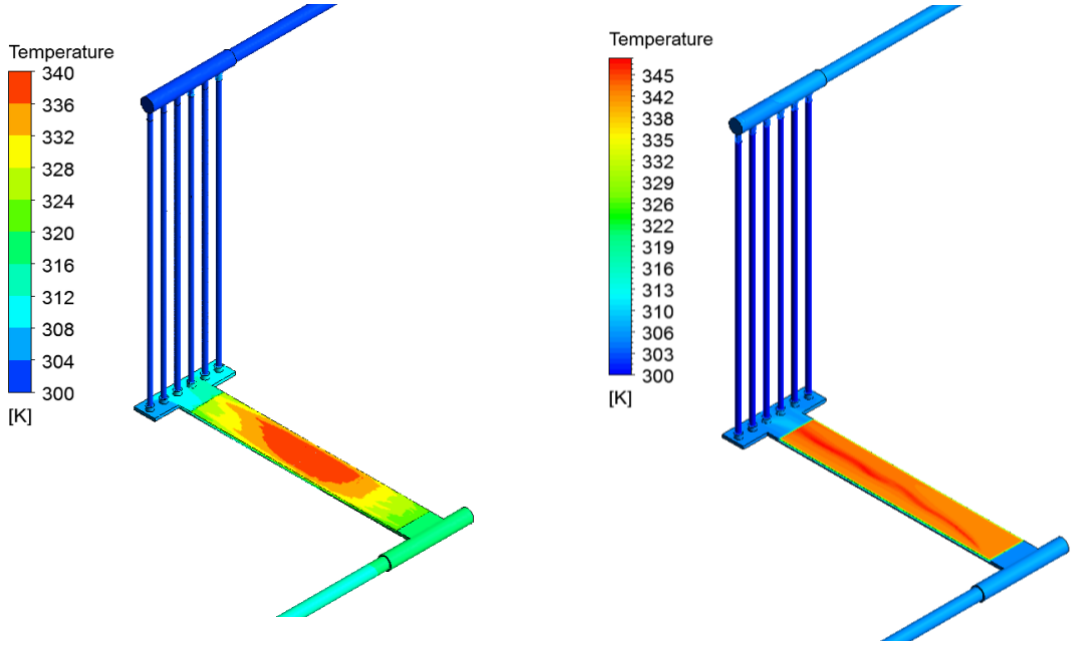

$A_0 = 0.08(m),\ f = 8(Hz)$

Figure 20. Effect of oscillatory frequency on the temperature contours

3.5. Effect of oscillatory amplitude:

The effect of oscillatory amplitude on the averaged surface temperature is shown in Figure 21 for oscillatory frequency 4 Hz. The figure shows that similar to the effect of the oscillatory frequency, increasing the amplitude also increases the heat transfer rate in the RMDHL loop. It worth to notice that in the conventional reciprocating driven mechanism, increasing the oscillatory amplitude requires a large cylinder and accordingly larger driving system. On the other hand, increasing the frequency of the driving mechanism should be analyzed carefully since the intense vibration without appropriate damping mechanism could result in mechanical failure of the electronic equipment.

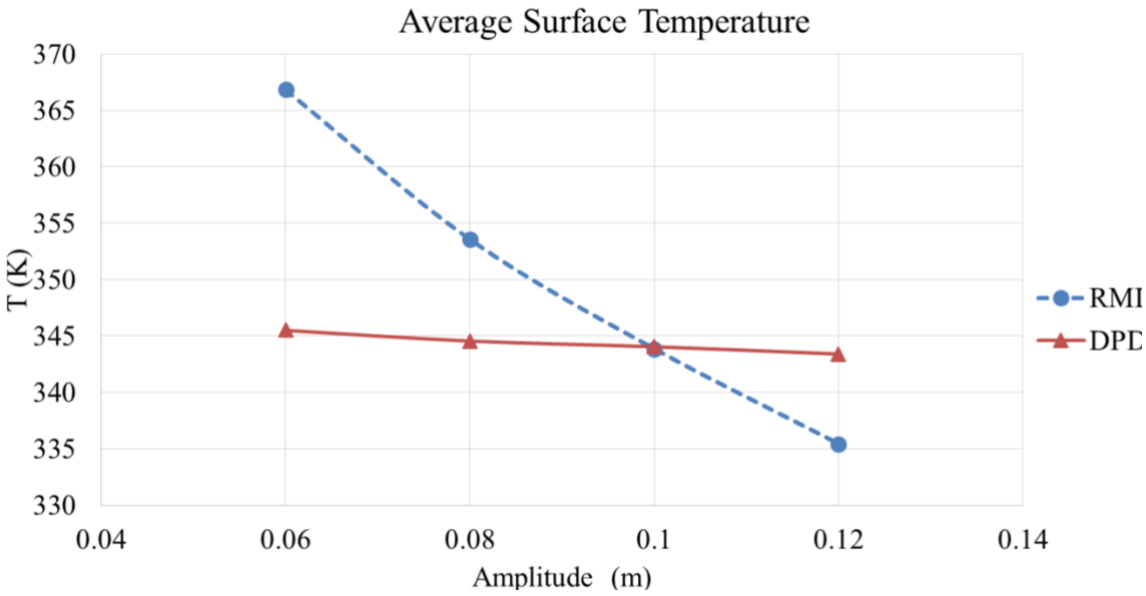

Figure 21. Effect of oscillatory amplitude on the averaged surface temperature

Figure 22 shows the effect of oscillatory amplitude on the temperature contours for the RMDHL and their comparison with the DPDHL loop. The figure also shows a more uniform surface temperature for the RMDHL compared to the DPDHL loop. The figure indicates that increases of the amplitude are less effective on the temperature uniformity of the surface compared to the oscillatory frequency in the RMDHL loops. Temperature contours for the DPDHL show a similar trend as in figure 5 since the flow rate of the cooling fluid was increased for both cases.

RMDHL

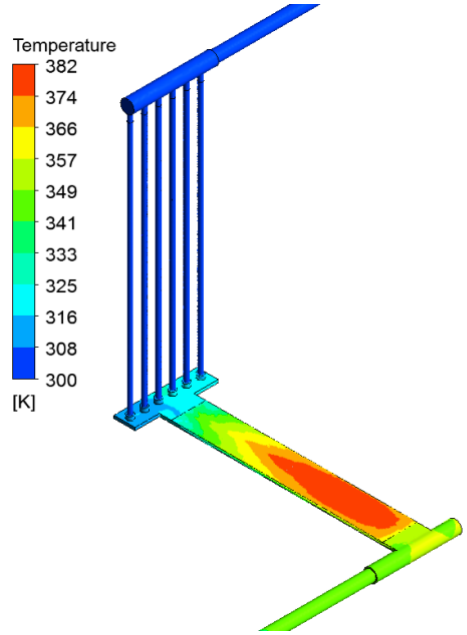

DPDHL

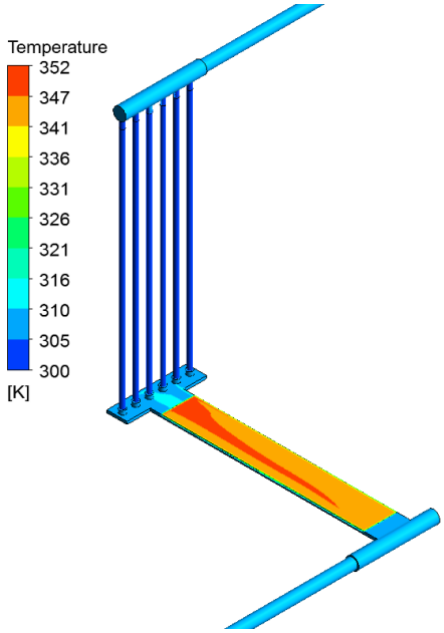

$$A_0 = 0.06(m),\ f = 4(Hz)$$

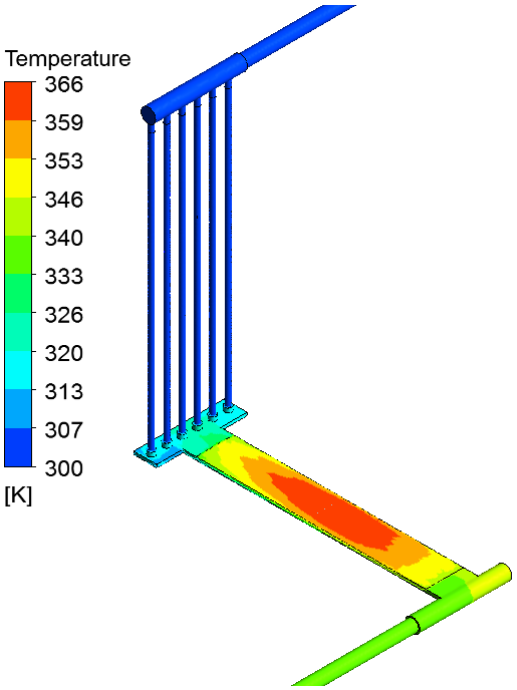

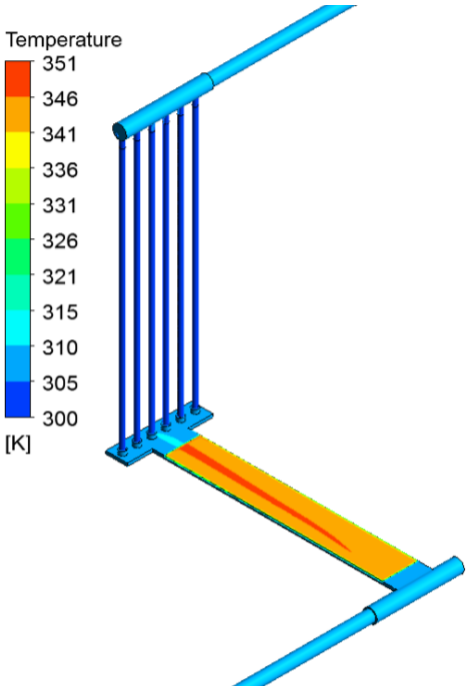

$$A_0 = 0.08(m),\ f = 4(Hz)$$

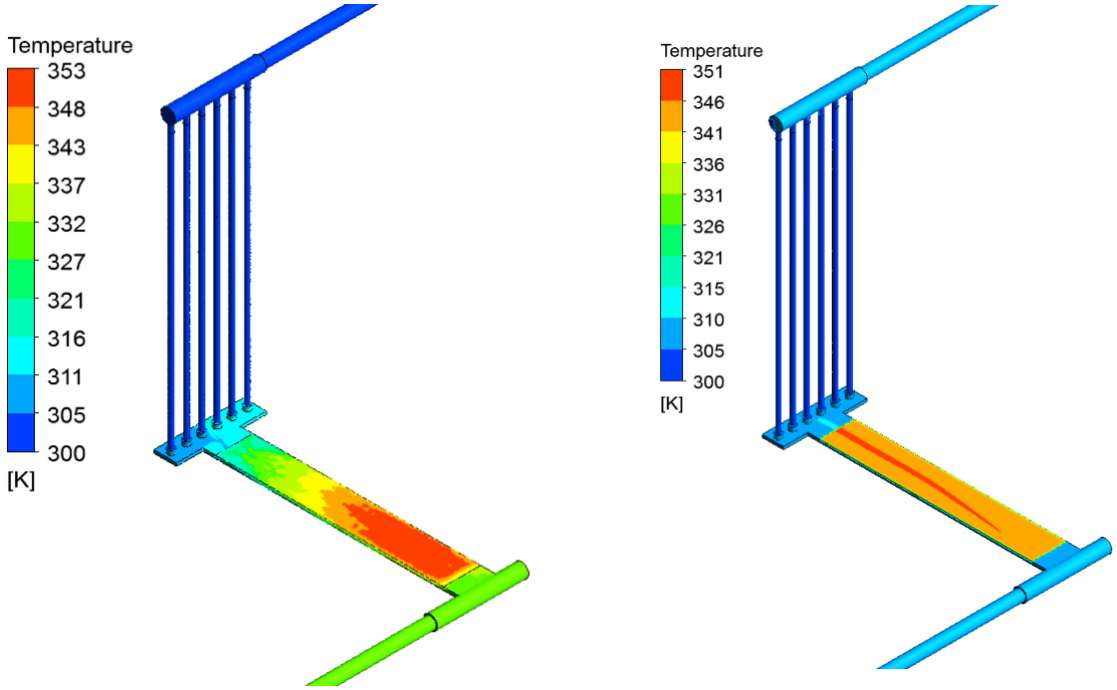

$$A_0 = 0.10(m),\ f = 4(Hz)$$

Figure 22. Effect of oscillatory amplitude on the temperature contours.

3.6. Nusselt number in the RMDH loop:

The overall Nusselt number for the RMDHL cooling loop is defined as:

$$Nu = \frac{h_a D_h}{k} \tag{12}$$

Where h_a is the overall heat transfer coefficient and can be calculated by:

$$h_a = \frac{Q}{A_w \Delta T_m} = \frac{\dot{Q}}{\left[T_{aw} - \frac{1}{2}\left(T_{in} + T_{out}\right)\right]} \tag{13}$$

where A_w is defined as the total area of the heated walls of the microchannels. $\dot{Q}$ is the surface heat flux and T_{aw} is the average wall temperature on the heated surface. T_{in} and T_{out} are the bulk temperatures of the working fluid at the two ends of the heated surface. k is the thermal conductivity, ρ is the density and c_p is the specific heat of water which are assumed to be constant.

Effect of oscillatory frequency and amplitude on the average Nusselt number of the RMDHL loop is shown in Figure 23. The figure shows the average Nusselt number increases almost linearly with the increase of both oscillatory amplitude and frequency. Contrary to the DPDHL loop in which the only controlling parameter on the heat transfer rate is the flow rate of the cooling liquid, the heat transfer rate of an RMDHL loop can be adjusted with both oscillatory frequency and amplitude. This would provide more flexibility for the design of the cooling system in different applications.

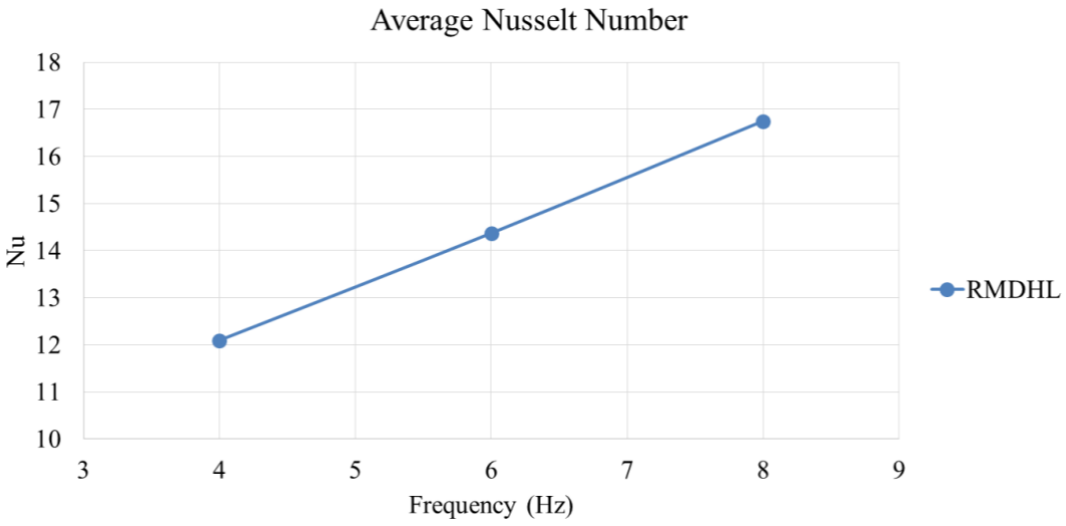

(a)

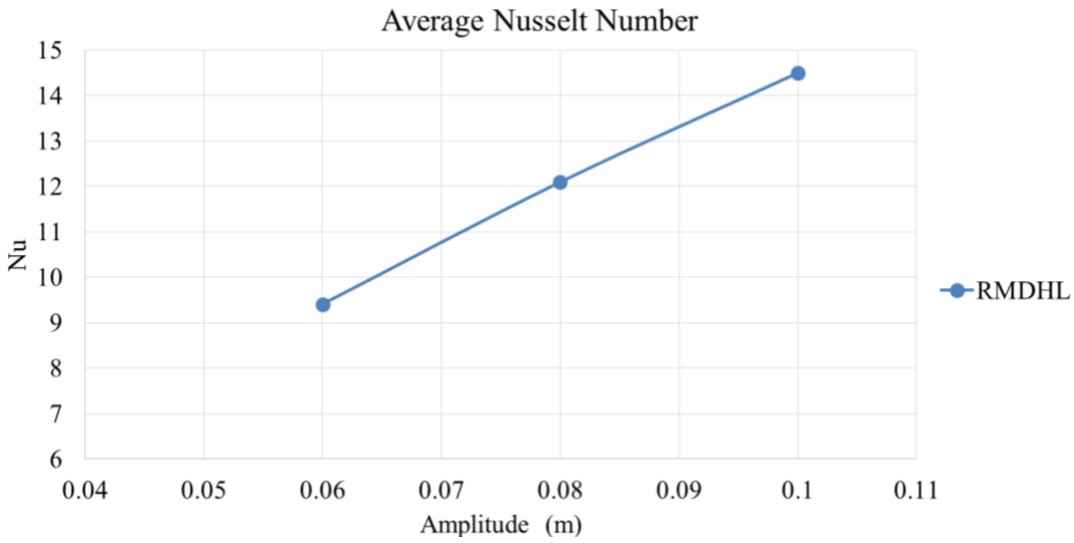

(b)

Figure 23. Average Nusselt number for different oscillatory frequency and amplitude

One of the most important limitations of RMDHL cooling systems is the total flow rate of the system in each cycle. This drawback makes the application of the cooling loop limited to the small-scale application such as chip and board cooling. For the systems with higher volumetric flow rate, check valves (2 position solenoid valves) can be used as illustrated in Figure 24. It should be mentioned, to the best of our knowledge, solenoid valves have not been used in RMDHL loops, although they may provide great advantages compared to the other reciprocating mechanism. They can be used in conjunction with a pump means retrofitting the current cooling system would be possible by using them. Moreover, the reciprocating loops with solenoid valves have no limitation regarding maximum flow rate will the other methods can only deliver a limited mass of cooling liquid depends on the size of their containers or pistons. Further investigation on the performance of an RMDHL cooling system for can help to expand the application of this cooling system in various industrial applications.

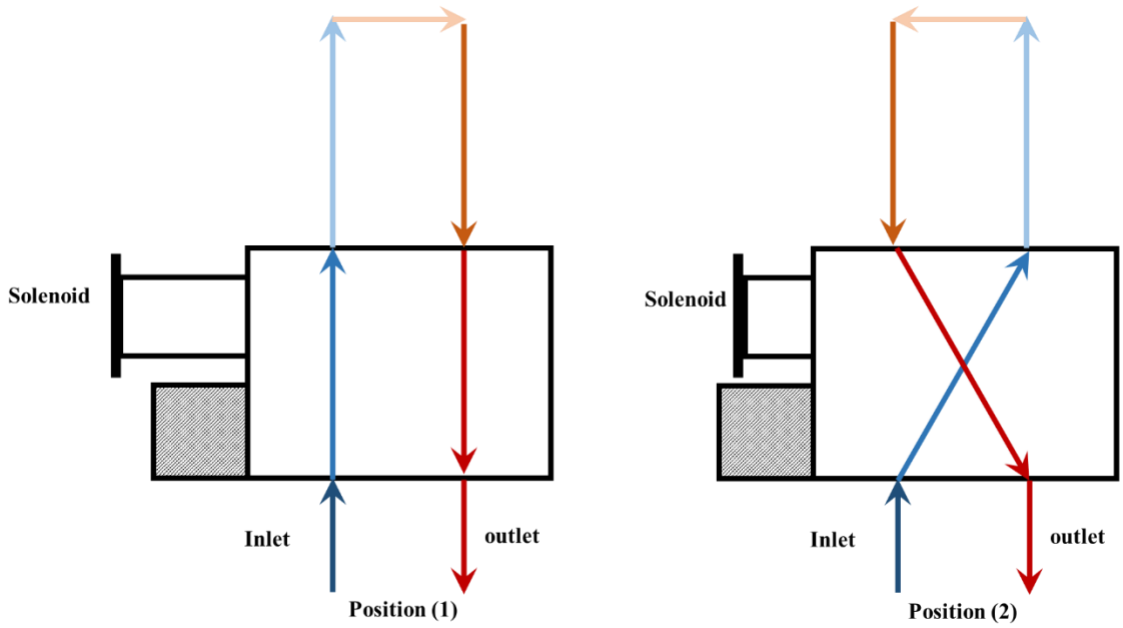

Figure 24. 4 way 2 position solenoid valves

4. Chapter 4: Experimental and Analytical Studies

4.1. Experiment setup

A bellows-type reciprocating heat transfer device was constructed for this study on the basis of Cao et al. [12]. Different components of the test rig are also illustrated in Appendix 1. The device is designed to handle high heat transfer rates with a single phase. A photo of the test setup, a CAD drawing of the reciprocating driver, and the locations of the thermocouples (102 to 107) are shown in Figure 25.

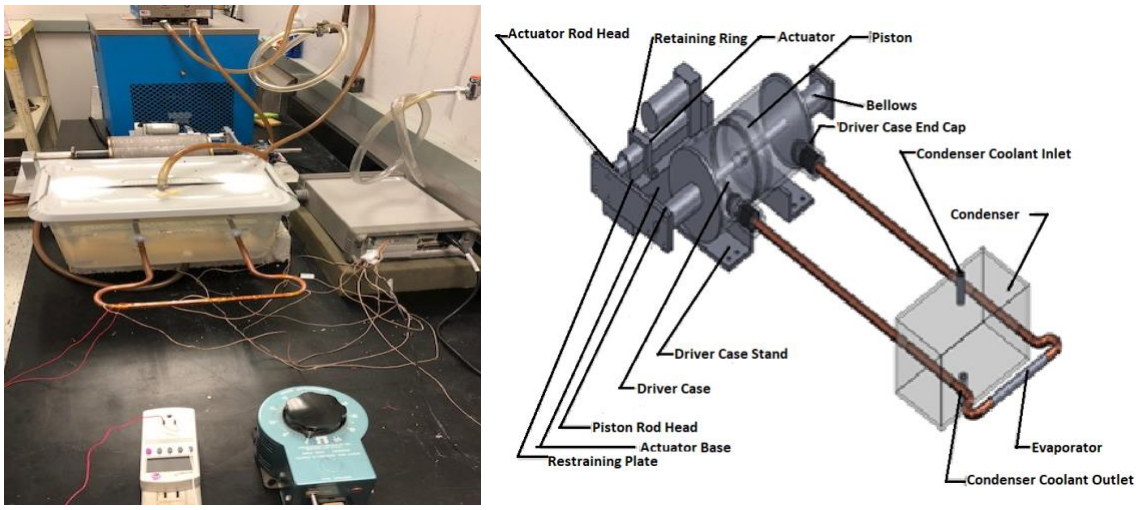

(a) (b)

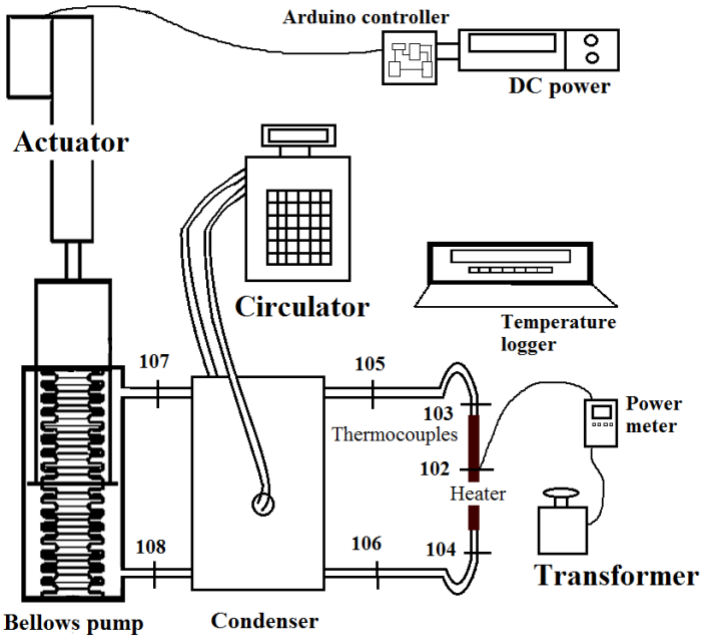

(c)

Figure 25. (a) Photo of the test rig assembly (b) Schematic representation of the test rig assembly (c) Location of the thermocouples [12]

The reciprocating driver includes a piston that is driven by an actuator in conjunction with two bellows for sealing purposes. The bellows are attached to the drive mechanism at each end of the chamber to facilitate a reciprocating motion of the piston while maintaining the chamber in a hermetic condition. The dimensions of the bellows are 50 turns with 2.70 cm inner diameter. The setup includes a flexible heater (KH-108 Omega lux flexible heater, 80 W), a Polystat thermal bath with the temperature range of -20oC to 150oC that supplies water with constant temperature for cooling the condenser, an Arduino controller that controls the driving mechanism, and a Progressive Automations Linear Actuator with a force of 150 lbs to drive the piston. A DC power supply regulated by a circuit board powers the actuator and to vary its reciprocating stroke/amplitude and frequency, an HP 34970A Data Acquisition unit records the temperatures at given points, a Staco Power regulator

connected to the flexible heaters was used to provide heat input to the evaporator section of the loop, and a P4400 Wattmeter was used to measure the heat input.

After turning on the constant temperature thermal bath and reaching the required cooling temperature, the operation of the linear actuator is initiated while the heat input to the evaporator heater gradually ramped to a test level. After the heat loop reaches a steady-state, the temperatures are recorded on the PC using the Agilent BenchLink Data Logger software. The reciprocating frequency, the stroke or amplitude of the reciprocating driver, heat transfer rate, the power input to the actuator, and the inlet cooling temperature of the condenser water were also recorded.

4.1.1 Results and discussion

The average temperature values in the condenser section, adiabatic section, and evaporator section are calculated using recorded thermocouples readings to study the effect of different operational parameters on the performance of the RMDHL:

$$T4\ (\text{condenser}) = 0.5 \times (T107 + T108)$$
$$T3\ (\text{adiabatic section}) = 0.5 \times (T105 + T106)$$
$$T2\ (\text{evaporator section}) = 0.5 \times (T103 + T104)$$
$$T1 = T102$$

where T102 to T108 are the temperatures recorded by the thermocouples located in the test rig according to Figure 25 (c).

The effect of the reciprocating amplitude on the temperature distribution in the RMDHL is shown in Figure 26 under the conditions of input power = 60 W, reciprocating frequency = 20 s/cycle, and cooling-water inlet temperature = 20^{o}C. The figure shows that as the amplitude of the reciprocating driver increases the loop surface temperature

decreases and the temperature uniformity along the loop improves. It is believed that an ideal cooling condition for the loop performance would exist when the heated fluid in the hot region could fully reach the cold part of the loop. However, if the reciprocating amplitude is less than the minimum requirement and the heated water could not effectively reach the cold region of the loop, the heat transfer rate would decrease and the temperature gradient would increase significantly.

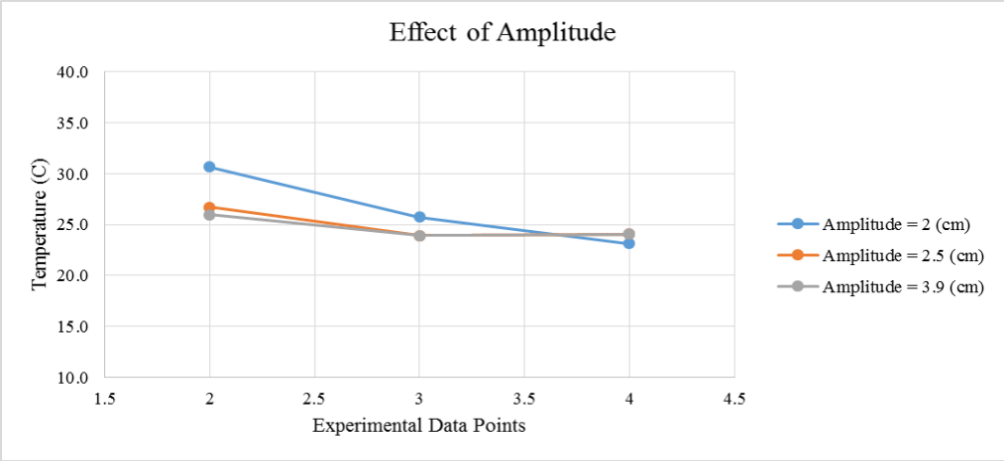

Figure 26. Effect of amplitude on the surface temperature of RMDHL

The effect of the reciprocating frequency in terms of time per cycle on the temperature distribution along the cooling loop is shown in Figure 27. As can be seen from the figure, with an input power =60 W, a water inlet cooling temperature = 20 ^{o}C, and a driver amplitude = 2.5 cm, both a higher frequency of 13 s/cycle and a lower frequency of 20 s/cycle result in a higher temperature gradient along the loop while a moderate frequency of 16 s/cycle produces a much more uniform temperature. In contrast to the effect of the amplitude, a higher frequency may not necessarily improve the temperature uniformity

although the temperature in the condenser section may be lower. Also, the temperature in the adiabatic section appears to be insensitive to the reciprocating frequency.

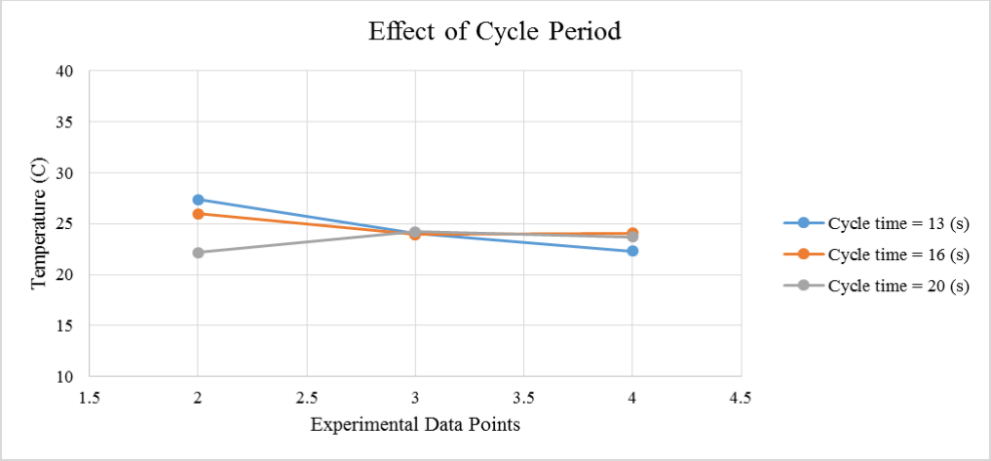

Figure 27. Effect of cycle period on the surface temperature of RMDHL

Figure 28 illustrates the effect of the inlet temperature of the cooling water on the surface temperature of the RMDHL for the temperature range of 15 to 30 ^{o}C. The input power, frequency, and amplitude are, respectively, set at 60 W, 16 s/cycle and 2.5 cm. Like many other heat transfer devices, the cooling water temperature controls the temperature level of the loop and a lower cooling water temperature produces a lower loop temperature level.

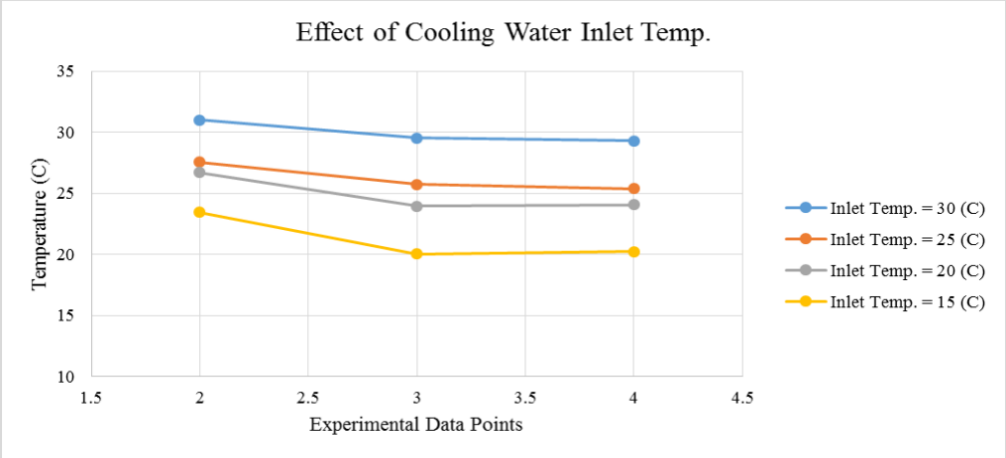

Figure 28 Effect of cooling water inlet temperature on the surface temperature of the RMDHL

With the cooling water at 20oC, frequency at 16 s/cycle, and amplitude at 2.5 cm, The effect of the input power to the flexible heater on the temperature distribution along the RMDHL is shown in Figure 29. As expected, a higher heat input would increase both the temperature level and temperature gradient along the loop. Also, the temperature gradient is primarily caused by heat transfer in the evaporator section. The temperature gradient from the adiabatic section to the condenser section is almost zero as evidenced by the almost identical readings of T4 and T3, due to the effective water cooling in the condenser section.

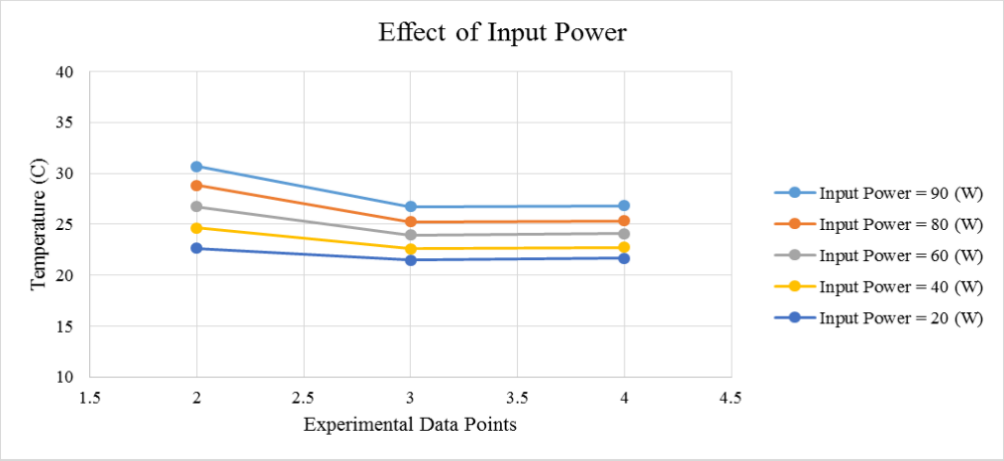

Figure 29 Effect of input power on the surface temperature of RMDHL

4.1.2 Effective heat transfer coefficient

The so-called effective heat transfer conductance has been evaluated for the system that is shown in Figure 30. Generally, it is used for a heat transfer device to gauge its performance, and is calculated by the following relation:

$$k_{eff} = \frac{QL}{A\Delta T} \tag{14}$$

where Q represents the heat input rate, L represents the effective distance between evaporative and condensation sections, ΔT is the temperature difference between the evaporative section and condensation section, and A is the cross-sectional area calculated based on the outer diameter of the loop tubing.

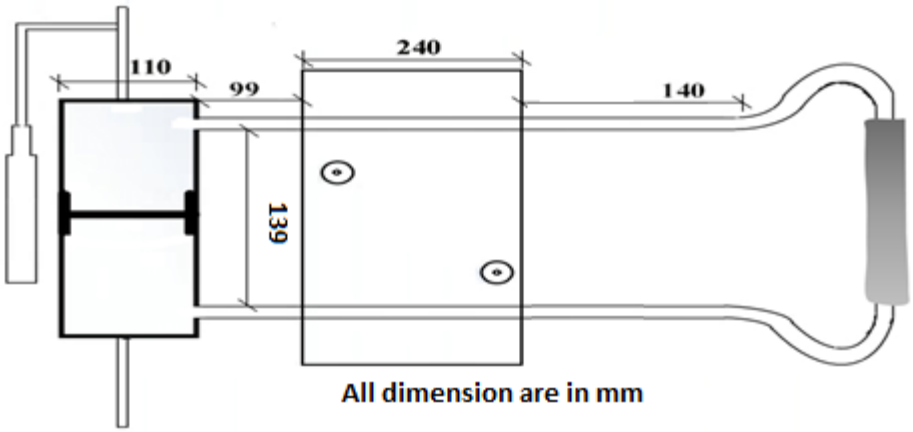

Figure 30. Experimental setup

A sample calculation for 40W heat input in the evaporative section is shown as follows:

$$k_{eff} = \frac{(40)(.565)}{(1.417\times10^{-4})(1.5)} = 106327.9 W/mk \tag{14}$$

If the thermal conductivity of copper is considered to be $400 W/mk$, then

$$\frac{k_{eff}}{k} = 265.81 \tag{15}$$

From the calculation, it is evidenced that the RMDHL of this study is an effective heat transfer device. For more general use of the experimental data of this study, a correlation has been developed based on the flow kinematic Reynolds number $\mathrm{Re}_{\omega} = \omega D^2/\nu$ and non-dimensional amplitude $A_0 = x/D$. Based on the experimental data, the following correlation equation for dimensionless effective heat transfer conductance is obtained:

$$\frac{k_{eff}}{k} = 413.23\,\mathrm{Re}_{\omega}^{-0.4840} A_0^{0.535} \qquad 14 < \mathrm{Re}_{\omega} < 30 \ and \ 2 < A_0 < 6 \tag{16}$$

4.2. Analytical Modelling

4.2.1. Power analysis for two-phase oscillating flow

This section presents a novel approach to analytically approximate the power consumption of a two-phase oscillating flow system using the RMDHL as a case study. A number of important aspects must be taken into consideration in designing the cooling system including a cold plate in accordance with the specifications of the thermal management system. These aspects include:

1. Working fluid displacement volume. A sufficiently large working fluid displacement volume, which is facilitated by the motion of the driver in a reciprocating cycle, is critical to ensuring adequate liquid supply from the condenser section to the evaporator section (cold plate) of the cooling loop. However, a larger displacement volume would require a larger size of the liquid reservoir and subsequently a larger cooling system. Therefore, a tradeoff must be made that would provide a sufficient displacement volume while maintaining the cooling system size at a reasonably low level.
2. Power consumption of the actuator. The cooling system of this project is an active cooling system that requires a certain amount of power input to overcome the frictional losses of the working fluid during the operation. A high-power consumption level, however, would not only affect the sustainability of the cooling system but also add additional cooling load requirement to the condenser of the system. Therefore, for a given amount of cooling load, the power consumption should be maintained at a low level.
3. Effective heat transfer in the evaporator and condenser. Effective heat transfer may be measured in terms of average heat transfer coefficients in both the evaporator and

condenser sections of the cooling loop. Since the maximum temperature drop between the surface being cooled and the coolant is limited to a certain value, a sufficiently high heat transfer coefficient is essential to reducing the temperature drop between the cooling channel surface and the coolant. A higher heat transfer coefficient would also result in a smaller condenser size, which has a significant impact on the displacement volume requirement.

4. Working fluid (coolant) selection. One of the critical requirements of the present system is the temperature uniformity in the evaporator section (cold plate) where the surface is being cooled. For this purpose, a working fluid that exhibits a smaller value of *dT/dp* under a two-phase saturated condition should be considered. Additionally, the cold plate is required to work at a rather low temperature. Therefore, a working fluid having a low melting temperature should be considered. Another requirement is a relatively low vapor pressure at the operating temperature of the cooling loop condenser for the consideration of the bellows design.

4.2.2. Working fluid displacement volume consideration.

4.2.2.1. Critical Displacement of the Reciprocating Driver

For a given reciprocating-mechanism driven heat loop, the volume displacement of the reciprocating driver must be sufficiently large so that the liquid can be supplied from the condenser section to the evaporator section. We wish to find a relationship that could describe this critical requirement for the operation of the cooling loop. Consider a cooling loop under a two-phase working condition (liquid and vapor coexist) similar to that schematically shown in Figure 31.

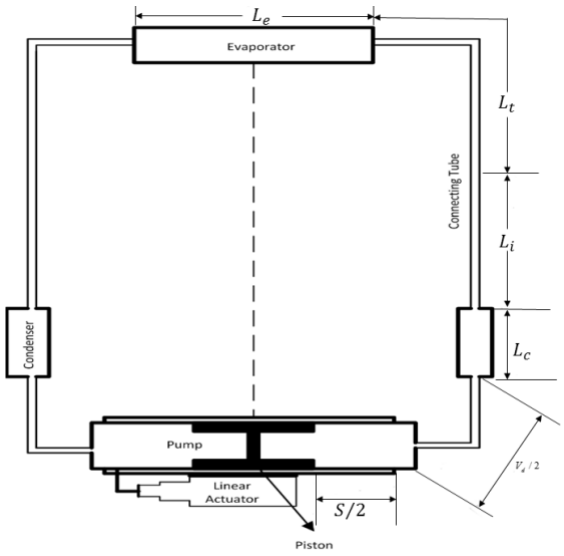

Figure 31. A linear-actuator operated reciprocating mechanism driven heat loop (RMDHL)

The cooling loop is assumed to have a condenser section on each side of the reciprocating driver, and the loop is symmetric about the line connecting the midpoints of the evaporator and reservoir. Because of this geometric symmetry, we would like to concentrate on the right half of the loop, as shown in Figure 31. The length and average interior cross-sectional area of the evaporator are denoted by L_e and A_e, respectively, the length and average interior cross-sectional area of the connecting tubing between the evaporator and the condenser are L_t and A_t, the length and interior cross-sectional area of each condenser section are L_c and A_c, the interior volume of the section between the end of the condenser and the piston right dead center is $V_d/2$, and the piston cross-sectional area and reciprocating stroke are A_p and S, respectively. The piston is stationed in the midsection of the liquid reservoir, and the vapor generated in the evaporator section pushes the liquid towards the condenser section with a liquid-vapor interface as indicated in the figure. Although there could be thin liquid films at the interior surface of the evaporator, the amount of liquid associated is neglected

in the current analysis. In the derivation of the critical liquid displacement, the critical working condition is assumed to be reached when the liquid at the center of the condenser, denoted by ***A*,** can just reach the midsection of the evaporator when the right-hand solenoid is turned on, and the piston reaches the right dead center in the reservoir. This condition means that the liquid initially at the condenser center would move to or pass the center of the evaporator as indicated in Figure 31, if the reciprocating-mechanism driven cooling loop would work adequately. A liquid balance between these two states would give the following relation:

$$A_p \frac{S}{2} + \frac{V_d}{2} + A_c L_c + A_t L_i \geq \frac{V_d}{2} + A_c L_c + A_t L_t + \frac{1}{2} A_e L_e + \frac{1}{2} A_c L_c + A_t L_i \tag{17}$$

Canceling out the common terms on both sides of the equation and multiplying the resulting equation by 2, we have

$$A_p S \geq A_c L_c + 2A_t L_t + A_e L_e \tag{18}$$

The above equation can be rewritten as:

$$A_p S \geq 2(\frac{1}{2} A_c L_c + A_t L_t + \frac{1}{2} A_e L_e) \tag{19}$$

The terms in the parentheses on the right-hand side of the above equation is the interior volume from the center of the condenser to the center of the evaporator on each side of the cooling loop, which reflects one of the essential geometric characteristics of the cooling loop in connection with the heat transfer distance and fluid displacement volume. If an effective displacement volume is defined for the entire cooling loop as follows:

$$V_{eff} = 2(\frac{1}{2} A_c L_c + A_t L_t + \frac{1}{2} A_e L_e) \tag{20}$$

(19) can be written as:

$$A_p S \geq V_{eff} \tag{21}$$

Equation (21) indicates that the liquid displacement volume of the piston as represented by A_pS must be equal to or greater than the effective displacement volume of the cooling loop if the cooling loop is to work properly.

In present experiment, the displacement volume is A_pS= 0.01026082*0.2=2.0521*10-3m3. On the other hand, effective displacement volume is V_{eff} =3.1185*10-4m3 which clearly satisfy the design requirement in Equation (21). However, is true only for a single-phase heat transfer mode. For a two-phase heat transfer mode, the criterion as represented by Equation (20) or Equation (21) is too conservative due to several reasons. Since the cross-sectional area of the reservoir is much greater than that of the rest of the cooling loop, the liquid velocity exiting the liquid reservoir should be relatively high. Even if the piston has reached the dead center in the reservoir, the liquid would continue to move towards the evaporator until the kinetic energy associated with it is exhausted. Additionally, once the liquid enters the evaporator section, some liquid will be evaporated into vapor. The evaporation will drastically change the volume of the flow stream and the liquid/vapor two-phase mixture will expand vigorously into the evaporator section. As a result, the section between the piston right dead center and the center of the evaporator in Figure 31 would be filled with both liquid and vapor, and the flow is in a two-phase flow condition. It is understood that the liquid fraction would change substantially along the loop. For the derivation of a more concise relation, an effective liquid fraction, ϕ, is used. By taking into account the two-phase flow condition, the liquid balance as represented by (17) should be modified as follows:

$$A_p \frac{S}{2} + \frac{V_d}{2} + \phi A_c L_c + \phi A_i L_i \geq \frac{V_d}{2} + \phi(A_c L_c + A_i L_t + \frac{1}{2} A_e L_e + \frac{1}{2} A_c L_c + A_i L_i) \quad (22)$$

Following the same deriving procedure, the following relation is obtained:

$$A_p S \geq 2(\frac{1}{2} A_c L_c + A_i L_t + \frac{1}{2} A_e L_e)\phi \quad (23)$$

Or

$$A_p S \geq \phi V_{eff} \quad (24)$$

The value of ϕ, by definition, is greater than zero and less than unity. The actual value of ϕ, however, has to be determined experimentally for most practical applications due to the complex heat transfer process in the cooling loop. Still, Equation (19) or (23) provides a concise criterion that could be used for the design of a heat loop. It should be pointed out that during the derivation of the above relations, the liquid reservoir is assumed to contain pure liquid and the backflow through the gap between the outer surface of the piston and the inner surface of the reservoir casing is neglected. If the reservoir would deal with a two-phase liquid-vapor mixture and the backflow effect is taken into account, the term A_pS in the above equations may need to be multiplied by a driver efficiency η that is less than unity:

$$\eta A_p S \geq 2\phi(\frac{1}{2} A_c L_c + A_i L_t + \frac{1}{2} A_e L_e) \quad (25)$$

The above equation may be rewritten in terms of the inner volumes of the condenser, tubing, and evaporator (V_c , V_t , and V_e , respectively) as follows:

$$\eta A_p S \geq 2\phi(\frac{1}{2} V_c + V_t + \frac{1}{2} V_e) \quad (26)$$

4.2.3. Power consumption of the actuator

4.2.3.1.Modeling and theoretical considerations

To facilitate the reciprocating motion of the working fluid in the loop, a sufficient amount of energy must be provided to overcome the frictional losses associated with the motion of the working fluid. This is achieved through the motion of a piston-driven by an actuator. Figure 32 shows the schematically the motion of the piston during a stroke from the left to the right of the reservoir. During this stroke, the actuator must overcome the pressure force difference between the frontal and back surfaces of the piston. The power consumption of the actuator or actuators may be calculated by the following relation:

$$P = (p_2 - p_1) A_p V_p = \Delta p A_p V_p \tag{27}$$

Where, p_1 is the average pressure on the back face of the piston, p_2 is the pressure on the frontal face of the piston, A_p is the cross-sectional area of the piston, and V_p is the velocity of the piston.

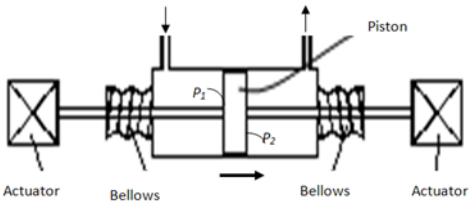

Figure 32. Motion of the piston in the reservoir

To simplify the problem, the concept of the mean effective velocity, similar to that in an internal combustion engine analysis, is employed. The mean effective velocity, $\overline{V}_p$, is directly related to the piston reciprocating frequency, *F*, by the following relation:

$$\bar{V}_p = 2S/(1/F) \tag{28}$$

In accordance with the mean effective velocity, the concept of the mean effective pressure difference is also employed in (27) for the power consumption of the actuator.

The pressure drop across the piston is also the pressure drop of the working fluid and may be calculated by using the concept of friction factor over a distance Δx:

$$\Delta p = f\frac{\rho u_m^2}{2D_h}\Delta x = f\frac{\Delta x}{2D_h}\rho\frac{(u_m\frac{\pi}{4}D_h^2\rho)^2}{(\frac{\pi}{4}D_h^2\rho)^2} = f(\frac{4}{\pi})^2\frac{\dot{m}^2\Delta x}{2D_h^5\rho} \tag{29}$$

Where $\dot{m}$ the mass flow is the rate of the fluid and D_h is the diameter or hydraulic diameter of the flow channel. Since the flow conditions are significantly different in individual sections of the evaporator, connection tubing, and condenser, the pressure drop in these sections will need to be calculated separately, and the total pressure drop is the summation of these individual pressure drops.

In calculating the pressure drop using (29), the friction factor, *f*, must be evaluated, which depends highly on the flow structure. In the present cooling loop consideration, the flow inside the flow channel is a complex liquid-vapor two-phase flow. Two commonly used flow models dealing with two-phase flows are homogenous flow model and separated flow model. In the homogenous flow model, the liquid and vapor phases are assumed to travel with the same velocity and mix well, while in the separated flow model, the liquid and vapor are assumed to display different properties and flow at different velocities. In general, the separated flow model may provide a better prediction with certainly added complexity. However, the homogeneous model works well when the flow velocity is high

so that the flow regime is either bubbly or misty flow. Since the flow velocity is relatively high in the present cooling loop, the homogeneous model is employed in the present design.

4.2.3.2.Mass flow rate induced by the motion of the piston

In the present cooling loop design, the piston/reservoir diameter may be in the range of 50 - 100 mm and piston stroke in the range of 50-80 mm. The piston reciprocating frequency may vary within a wide range. For the present two-phase application, the heat transfer is primarily due to phase change, and subsequently, the mass supply requirement to the cold plate is drastically reduced as compared to a single-phase flow. Therefore, the piston may operate at a low frequency. A low frequency will also reduce the power consumption of the actuator. If the piston diameter is taken to be 80 mm, the piston stroke to be 60 mm and the frequency to be 0.2 s^{-1}, the piston speed according to (28) would be:

$$\overline{V}_p = 2S/(1/F) = 2\times 0.06/(1/0.2) = 0.024 \text{m/s}$$

When R-11 is used, the corresponding mass flow rate is

$$\dot{m} = \rho_l A_p \overline{V}_p = 1440 \times \frac{\pi}{4} 0.08^2 \times 0.024 = 0.174 \text{ kg/s}$$

The friction coefficient may be evaluated using the following correlation [20]:

$$\left(\overline{C}_{f,e}\right)_m = \frac{3.774}{A_o\left(\text{Re}_\omega^{0.543} - 2.20863\right)} \tag{30}$$

Where c_f is the friction coefficient that is related to the friction factor by $f = 4c_f$. The Reynolds number in (30) is based on the mixture density and viscosity:

$$\text{Re} = \frac{VD_h\rho}{\mu}, \quad \frac{1}{\rho} = \frac{x}{\rho_v} + \frac{1-x}{\rho_l}, \quad \mu = \frac{x}{\mu_v} + \frac{1-x}{\mu_l}$$

For R-11 at 40oC, $\rho_l = 1440$ kg/m3, $\rho_v = 9.7$ kg/m3, $\mu_l = 3.75\times10^{-4}$ N-s/m2, $\mu_v = 1.19\times10^{-5}$ N-s/m2

4.2.3.3.Pressure drop in the evaporator section of the cooling loop

In this exemplary calculation, the effective quality in the evaporator is taken to be x = 0.5. Sufficiently low vapor quality is essential to keep the surface wall wetted and promote boiling heat transfer, which may be achieved once the requirement for liquid volume displacement is met. With the specified quality, the properties associated with the two-phase flow may be evaluated:

$$\rho = (\frac{0.5}{9.7} + \frac{1-0.5}{1440})^{-1} = 19.27\ kg/m^3$$

$$\mu = (\frac{0.5}{1.19\times10^{-5}} + \frac{1-0.5}{3.75\times10^{-4}})^{-1} = 2.31\times10^{-5}\ N\cdot s/m^2$$

$$\mathrm{Re} = \frac{VD_h\rho}{\mu} = \frac{4\dot{m}}{\pi D_h\mu} = \frac{4\dot{m}}{\pi\frac{2wh}{(w+h)}\mu} = \frac{4\times(0.174/6)}{\pi\times0.0084\times2.31\times10^{-5}} = 1.9\times10^5$$

Therefore, through (30),

$c_f = 0.0039$, $f = 4\times c_f = 0.0158$

and then the pressure drop across the cold plate is calculated:

$$\Delta p = f(\frac{4}{\pi})^2\frac{\dot{m}^2\Delta x}{2D_h^5\rho} = 0.0158\times(\frac{4}{\pi})^2\frac{(0.174/6)^2\times0.2}{2\times0.0084^5\times12.1} = 4256.8\ \mathrm{Pa}$$

4.2.3.4.Pressure drop in the connection tubing of the cooling loop

Since the size of the connection tubes is not subjected to serious limitations other than the displacement volume requirement, a larger diameter, 12 mm, herein is used to reduce the pressure drop. In this calculation, a vapor quality of 0.5 is used to reflect the fact that at a given time one leg of the connection tube may be filled substantially with liquid, while the

other leg may be filled substantially with vapor. The total connection tube length is taken to be 1 m with each leg being 0.5 m.

$$\rho = (\frac{0.5}{9.7} + \frac{1-0.5}{1440})^{-1} = 19.27\ kg/m^3$$

$$\mu = (\frac{0.5}{1.19\times10^{-5}} + \frac{1-0.5}{3.75\times10^{-4}})^{-1} = 2.31 = \times10^{-5}\ N\cdot s/m^2$$

$$\mathrm{Re} = \frac{VD_h\rho}{\mu} = \frac{4\dot{m}}{\pi D_h\mu} = \frac{4\times(0.174)}{\pi\times0.012\times2.31\times10^{-5}} = 8.0\times10^5$$

Therefore

$$c_f = 0.003,\ f = 4\times c_f = 0.012$$

$$\Delta p = f(\frac{4}{\pi})^2\frac{\dot{m}^2\Delta x}{2D_h^5\rho} = 0.012\times(\frac{4}{\pi})^2\frac{(0.174)^2\times1.0}{2\times0.012^5\times19.27} = 61416Pa$$

4.2.3.5.Pressure drop in the condenser section of the heat loop

For condenser design, an arrangement of 12 tubes having an inner diameter of 7 mm that are connected in parallel is considered. The tube length based on the total interior condenser volume as calculated before is 0.34 m. The vapor quality is taken to be 0.2, reflecting a much large percentage of liquid present in the condenser. Accordingly,

$$\rho = (\frac{0.2}{9.7} + \frac{1-0.2}{1440})^{-1} = 47.23\ kg/m^3$$

$$\mu = (\frac{0.2}{1.19\times10^{-5}} + \frac{1-0.2}{3.75\times10^{-4}})^{-1} = 5.28\times10^{-5}\ N\cdot s/m^2$$

$$\mathrm{Re} = \frac{VD_h\rho}{\mu} = \frac{4\dot{m}}{\pi D_h\mu} = \frac{4\times(0.174/12)}{\pi\times0.007\times5.28\times10^{-5}} = 5.0\times10^4$$

Therefore, $c_f = 0.0052$, $f = 4\times c_f = 0.0210$

$$\Delta p = f(\frac{4}{\pi})^2\frac{\dot{m}^2\Delta x}{2D_h^5\rho} = 0.021\times(\frac{4}{\pi})^2\frac{(0.174/12)^2\times0.34}{2\times0.007^5\times47.23} = 1532.90Pa$$

4.2.3.6.Total pressure drop in the heat loop

The total pressure drop in the cooling loop is the summation of individual pressure drops,

$$\Delta p_t = \Delta p_e + \Delta p_t + \Delta p_c = 4256.8 + 61416 + 1532.9 = 67205.7 \text{ Pa}$$

The power consumption is:

$$P = \Delta p_t A_p \overline{V}_p = 67205.7 \times \frac{\pi}{4} 0.08^2 \times 0.024 = 8.11 \text{W}$$

The average force acting on the piston is

$$F = \Delta p_t A_p = 66855.5 \times \frac{\pi}{4} 0.08^2 = 337.8 N$$

5. Chapter 5: Conclusion and future recommendations

5.1. Conclusion

The numerical results of this study showed that the novel numerical method using a dynamic mesh technique has successfully overcome the difficulties associated with conventional methods in handling the flow boundary conditions of reciprocating flow to produce accurate and verified simulation results. Using the developed numerical method, the performance of a reciprocating-mechanism driven heat loop (RMDHL) was compared with a conventional dynamic-pump driven heat loop (DPDHL) for heat transfer and surface temperature uniformity. The effects of the oscillatory amplitude and frequency on the Nusselt number and surface temperature for a liquid assisted cooling system have been studied. The results showed that the RMDHL provides superior cooling performance compared to the conventional DPDHL cooling systems. The reciprocating flow provided a more uniform and lower surface temperature for the system when the oscillatory frequency was large enough. For the present system, the obtained results also indicated that the average Nusselt number increases almost linearly with the oscillatory frequency and amplitude for the range of the investigation.

In the experimental study, the performance of a reciprocating cooling loop and the effect of different parameters on its performance has been studied. The experimental studies have produced detailed results for heat transfer rate and temperature distribution as a function of reciprocating amplitude, frequency, cooling water temperature, heat input to the evaporator, and power consumption of the driver. The results showed that as the amplitude of the reciprocating flow increases the loop surface temperature decreases and the

temperature uniformity along the loop improves. However, in contrast to the effect of the amplitude, a higher frequency may not necessarily improve the temperature uniformity although the temperature in the condenser section may be lower. Also, the temperature in the adiabatic section appears to be insensitive to the reciprocating frequency. The experimental results were then summarized in a semi-empirical correlation that provides a useful design tool for the thermal engineer community.

Finally, the derived analytical solutions for the critical displacement volume and the power consumption of the reciprocating driver have been verified through the experimental data of this study as well as prior studies. The analytical results clearly illustrated what important critical requirements should be considered in designing an RMDHL system and how the power consumption of the reciprocating driver could be reduced.

5.2. Future recommendation

Although the reciprocating-mechanism driven heat loop (RMDHL) has the advantages of achieving a high heat flux removal level and temperature uniformity as compared to the conventional dynamic-pump driven heat loop (DPDHL), the required driver displacement volume may be large, which requires a substantially large driver chamber. For relatively low heat flux or long-distance heat transfer applications, the advantages of the RMDHL for ground applications may be somewhat reduced. A future study in this area should attempt to find a way to reduce the displacement volume while maintaining high heat flux removal level, temperature uniformity, and cavitation free characteristics.

References

[1] Z. Zuo, L. Hoover, and A. Phillips, “An integrated thermal architecture for thermal management of high power electronics,” in *Thermal Challenges in Next Generation Electronic Systems*, 2002, pp. 317–336.

[2] A. Bergles, “High-flux processes through enhanced heat transfer,” *ICBHT*, pp. 1–13, 2003.

[3] Z. Liu, S. Tan, H. Wang, Y. Hua, and A. Gupta, “Compact thermal modeling for packaged microprocessor design with practical power maps,” *Integr. VLSI J.*, vol. 47, no. 1, pp. 71–85, Jan. 2014, doi: 10.1016/j.vlsi.2013.07.003.

[4] K. Vafai, “High heat flux electronic cooling apparatus, devices and systems incorporating same,” US 20020135980A1, 2002.

[5] G. Hetsroni, A. Mosyak, and Z. Segal, “Nonuniform temperature distribution in electronic devices cooled by flow in parallel microchannels,” *IEEE Trans. Components Packag. Technol.*, vol. 24, no. 1, pp. 16–23, 2001, doi: 10.1109/6144.910797.

[6] W. Jeakins and W. Moizer, “Cooling of electronic equipment,” *US Pat. 6,538,881*, pp. 1–70, 2003.

[7] S. Krishnamoorthy, “Modeling and Analysis of Temperature Distribution in Nanoscale Circuits and Packages,” University of Illinois at Chicago, 2008.

[8] W. Wu, S. Wang, W. Wu, K. Chen, S. Hong, and Y. Lai, “A critical review of battery thermal performance and liquid based battery thermal management,” *Energy Convers. Manag.*, vol. 182, no. January, pp. 262–281, 2019, doi: 10.1016/j.enconman.2018.12.051.

[9] L. Huat, Y. Ye, and A. A. O. Tay, “Integration issues of lithium-ion battery into electric vehicles battery pack,” *J. Clean. Prod.*, vol. 113, pp. 1032–1045, 2016, doi: 10.1016/j.jclepro.2015.11.011.

[10] T. Salamon, R. L. Amalfi, N. Lamaison, J. B. Marcinichen, and J. R. Thome, “Two-phase liquid cooling system for electronics, part 1: Pump-driven loop,” *Proc. 16th Intersoc. Conf. Therm. Thermomechanical Phenom. Electron. Syst. ITherm 2017*, no. August, pp. 667–677, 2017, doi: 10.1109/ITHERM.2017.7992551.

[11] Y. Cao and M. Gao, “Experimental and Analytical Studies of Reciprocating-Mechanism Driven Heat Loops (RMDHLs),” *J. Heat Transfer*, vol. 130, no. 7, p. 072901, 2008, doi: 10.1115/1.2909078.

[12] Y. Cao, D. Xu, and M. Gao, “Experimental study of a bellows-type reciprocating-mechanism driven heat loop,” *Int. J. Energy Res.*, vol. 37, no. 6, pp. 665–672, May 2013, doi: 10.1002/er.2889.

[13] Y. Cao and M. Gao, “Reciprocating-Mechanism Driven Heat Loops and Their Applications,” *ASME J. Heat Transf.*, vol. Volume 1, pp. 781–789, Jul. 2003, doi: 10.1115/HT2003-47195.

[14] J. Anderson, “Ludwig Prandtl ’ s Boundary Layer,” *Phys. Today*, no. December, pp. 42–48, 2005.

[15] G. Xiao, T. Zhou, M. Ni, C. Chen, Z. Luo, and K. Cen, “Study on oscillating flow of moderate kinetic Reynolds numbers using complex velocity model and phase Doppler anemometer,” *Appl. Energy*, vol. 130, pp. 830–837, 2014, doi: 10.1016/j.apenergy.2014.02.005.

[16] Z. Yu, X. Mao, and A. J. Jaworski, “Experimental study of heat transfer in oscillatory gas flow inside a parallel-plate channel with imposed axial temperature gradient,” *Int. J. Heat Mass Transf.*, 2014, doi: 10.1016/j.ijheatmasstransfer.2014.06.031.

[17] T. Zhao and P. Cheng, “A numerical solution of laminar forced convection in a heated pipe subjected to a reciprocating flow,” *Int. J. Heat Mass Transf.*, vol. 38, no. 16, pp. 3011–3022, 1995, doi: 10.1016/0017-9310(95)00017-4.

[18] C. Walther, H.-D. Kühl, T. Pfeffer, and S. Schulz, “Influence of developing flow on the heat transfer in laminar oscillating pipe flow,” *Forsch. im Ingenieurwes.*, vol. 64, no. 3, pp. 55–63, 1998, doi: 10.1007/PL00010849.

[19] C. Sert and A. Beskok, “Numerical Simulation of Reciprocating Flow Forced Convection in Two-Dimensional Channels,” *J. Heat Transfer*, vol. 125, no. 3, pp. 403–412, 2003, doi: 10.1115/1.1565092.

[20] T. S. Zhao and P. Cheng, “Experimental studies on the onset of turbulence and frictional losses in an oscillatory turbulent pipe flow,” *Int. J. Heat Fluid Flow*, vol. 17, no. 4, pp. 356–362, 1996, doi: 10.1016/0142-727X(95)00108-3.

[21] R. Mahamud and C. Park, “Reciprocating air flow for Li-ion battery thermal management to improve temperature uniformity,” *J. Power Sources*, vol. 196, no. 13, pp. 5685–5696, 2011, doi: 10.1016/j.jpowsour.2011.02.076.

[22] P. Bouvier, P. Stouffs, and J. P. Bardon, “Experimental study of heat transfer in oscillating flow,” *Int. J. Heat Mass Transf.*, vol. 48, no. 12, pp. 2473–2482, 2005, doi: 10.1016/j.ijheatmasstransfer.2005.01.037.

[23] M. R. Mackley and P. Stonestreet, “Heat transfer and associated energy dissipation for oscillatory flow in baffled tubes,” *Chem. Eng. Sci.*, vol. 50, no. 14, pp. 2211–2224, 1995, doi: 10.1016/0009-2509(95)00088-M.

[24] O. Popoola, A. Bamgbade, and Y. Cao, “A Numerical Model of a Reciprocating-Mechanism Driven Heat Loop for Two-Phase High Heat Flux Cooling,” *J. Therm. Sci. Eng. Appl.*, vol. 8, no. 4, pp. 41006–41018, Jul. 2016.

[25] U. Akdag and A. F. Ozguc, “Experimental investigation of heat transfer in oscillating annular flow,” *Int. J. Heat Mass Transf.*, vol. 52, no. 11–12, pp. 2667–2672, 2009, doi: 10.1016/j.ijheatmasstransfer.2009.01.006.

[26] M. D. Alam, S. T. Hossain, H. S. Simanto, M. Shoyeb, and U. Mithu, “Experimental and Numerical Investigation of an Air to Water Heat Exchanger,” in *International Conference on Mechanical, Industrial and Energy Engineering*, 2014, pp. 1–5.

[27] K. Young, C. Wang, L. Y. Wang, and K. Strunz, *Electric Vehicle Integration into Modern Power Networks*. 2013.

[28] Z. Rao and S. Wang, “A review of power battery thermal energy management,” *Renew. Sustain. Energy Rev.*, vol. 15, no. 9, pp. 4554–4571, Dec. 2011, doi: 10.1016/j.rser.2011.07.096.

[29] A. A. Pesaran, G. H. Kim, and M. Keyser, “Integration issues of cells into battery packs for plug-in and hybrid electric vehicles,” *24th Int. Batter. Hybrid Fuel Cell Electr. Veh. Symp. Exhib. 2009, EVS 24*, vol. 3, no. January, pp. 1924–1930, 2009.

[30] L. Zhou, Y. Zheng, M. Ouyang, and L. Lu, “A study on parameter variation effects on battery packs for electric vehicles,” *J. Power Sources*, vol. 364, pp. 242–252, 2017, doi: 10.1016/j.jpowsour.2017.08.033.

[31] M. Hoh, J. Fuhr, C. Kuper, and G. Houchin-Miller, “Thermal Management of Hybrid Vehicle Battery Systems,” pp. 1–10, 2009.

[32] “Comparing layout of the Soul EV battery with other EVs,” 2016. [Online]. Available: http://www.mykiasoulev.com/forum/viewtopic.php?t=662.

[33] W. B. Gu and C. Y. Wang, “Thermal-Electrochemical Modeling of Battery Systems,” *J. Electrochem. Soc.*, vol. 147, no. 8, p. 2910, 2000, doi: 10.1149/1.1393625.

[34] J. Kim, J. Oh, and H. Lee, “Review on battery thermal management system for electric vehicles,” *Appl. Therm. Eng.*, vol. 149, no. December 2018, pp. 192–212, 2019, doi: 10.1016/j.applthermaleng.2018.12.020.

[35] L. H. Saw, A. A. O. Tay, and L. W. Zhang, “Thermal management of lithium-ion battery pack with liquid cooling,” *Annu. IEEE Semicond. Therm. Meas. Manag. Symp.*, vol. 2015-April, no. March, pp. 298–302, 2015, doi: 10.1109/SEMI-THERM.2015.7100176.

[36] A. A. Pesaran and M. Keyser, “Thermal characteristics of selected EV and HEV batteries,” *Sixt. Annu. Batter. Conf. Appl. Adv. Proc. Conf. (Cat. No.01TH8533)*, pp. 219–225, 2001, doi: 10.1109/BCAA.2001.905129.

[37] G. Xia, L. Cao, and G. Bi, “A review on battery thermal management in electric vehicle application,” *J. Power Sources*, vol. 367, pp. 90–105, 2017, doi: 10.1016/j.jpowsour.2017.09.046.

[38] S. Wang, K. Li, Y. Tian, J. Wang, Y. Wu, and S. Ji, “Improved thermal performance of a large laminated lithium-ion power battery by reciprocating air flow,” *Appl. Therm. Eng.*, vol. 152, no. February, pp. 445–454, 2019, doi: 10.1016/j.applthermaleng.2019.02.061.

[39] H. Teng and K. Yeow, “Design of direct and indirect liquid cooling systems for high-capacity, high-power lithium-ion battery packs,” *SAE Int. J. Altern. Powertrains*, vol. 1, no. 2, pp. 525–536, 2012, doi: 10.4271/2012-01-2017.

[40] Y. Zhao, B. Zou, C. Li, and Y. Ding, “Active cooling based battery thermal management using composite phase change materials,” *Energy Procedia*, vol. 158, pp. 4933–4940, 2019, doi: 10.1016/j.egypro.2019.01.697.

[41] F. Bai, M. Chen, W. Song, Z. Feng, Y. Li, and Y. Ding, “Thermal management performances of PCM/water cooling-plate using for lithium-ion battery module based on non-uniform internal heat source,” *Appl. Therm. Eng.*, vol. 126, pp. 17–27, 2017, doi: 10.1016/j.applthermaleng.2017.07.141.

[42] T. L. Bergman and F. P. Incropera, *Fundamentals of heat and mass transfer*. John Wiley & Sons, Ltd, 2011.

Appendix

Polystat thermal bath
(-20oC to 150oC)

P4400 Wattmeter (max power 1800W)

Staco Power regulator (0-120)V

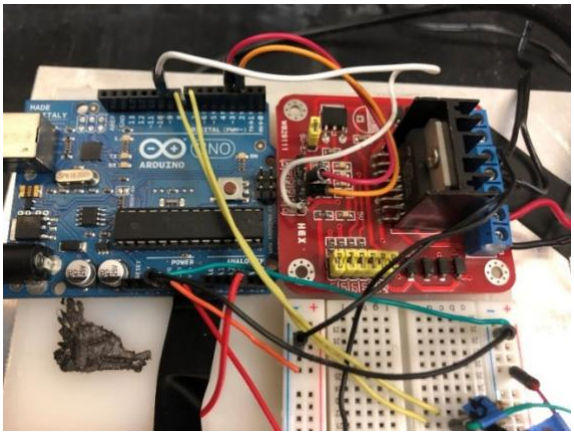

Arduino controller

HP 34970A Data acquisition unit

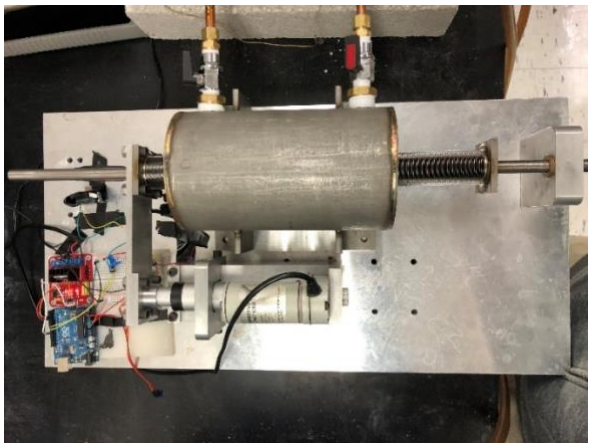

Oscillating cooling pump

Omega Thermocouple K type

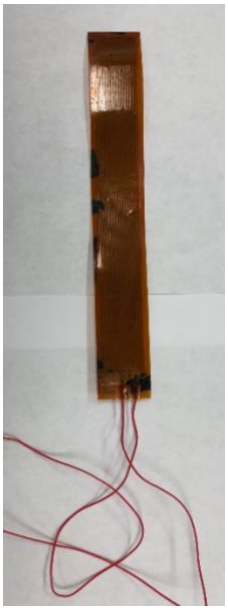

KH-108 Omega lux flexible heater (80 W)

Progressive Automations Linear Actuator (force: 150 lbs.)

Cold plate main plate

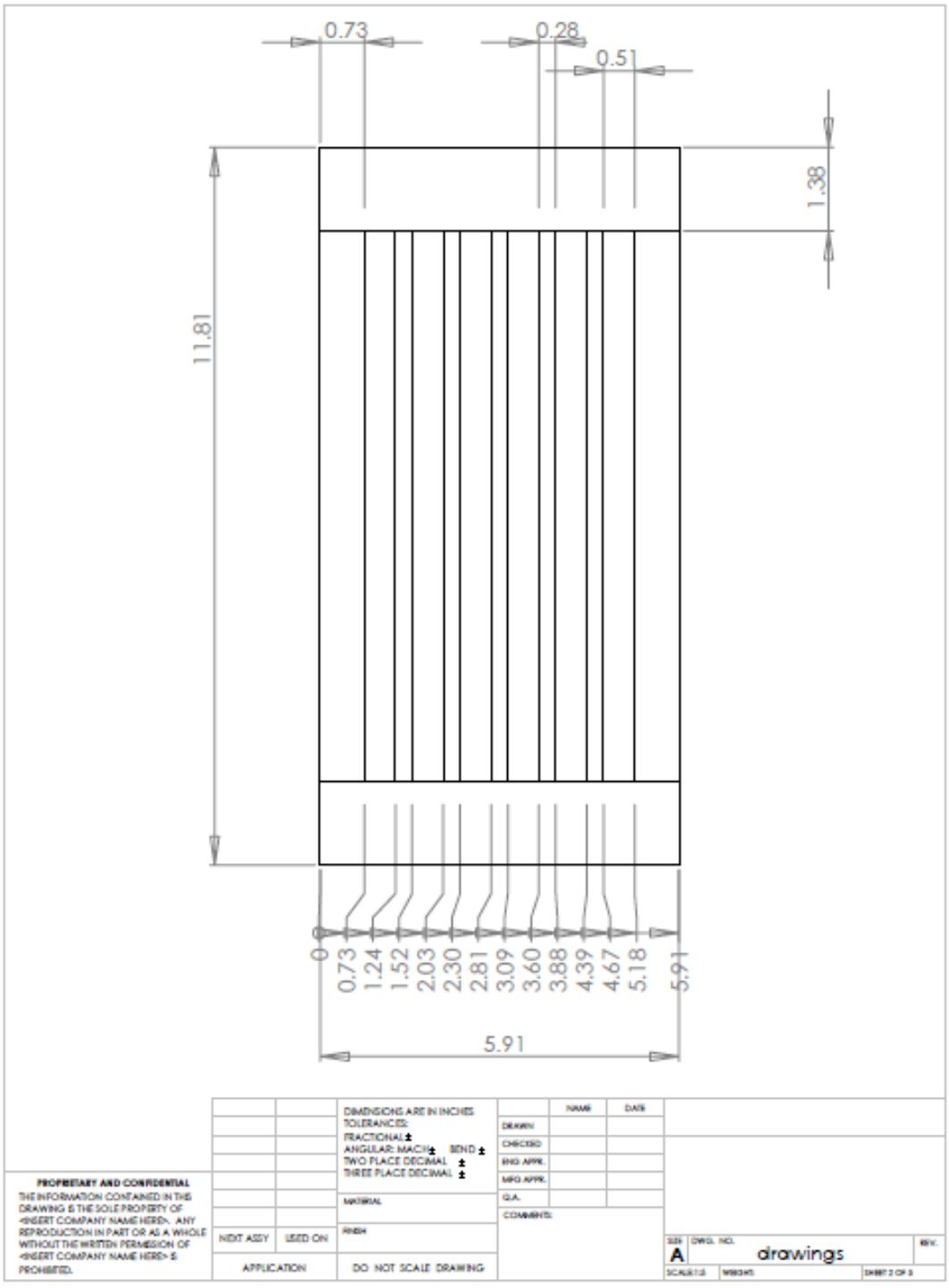

Cold plate assembly sectional view

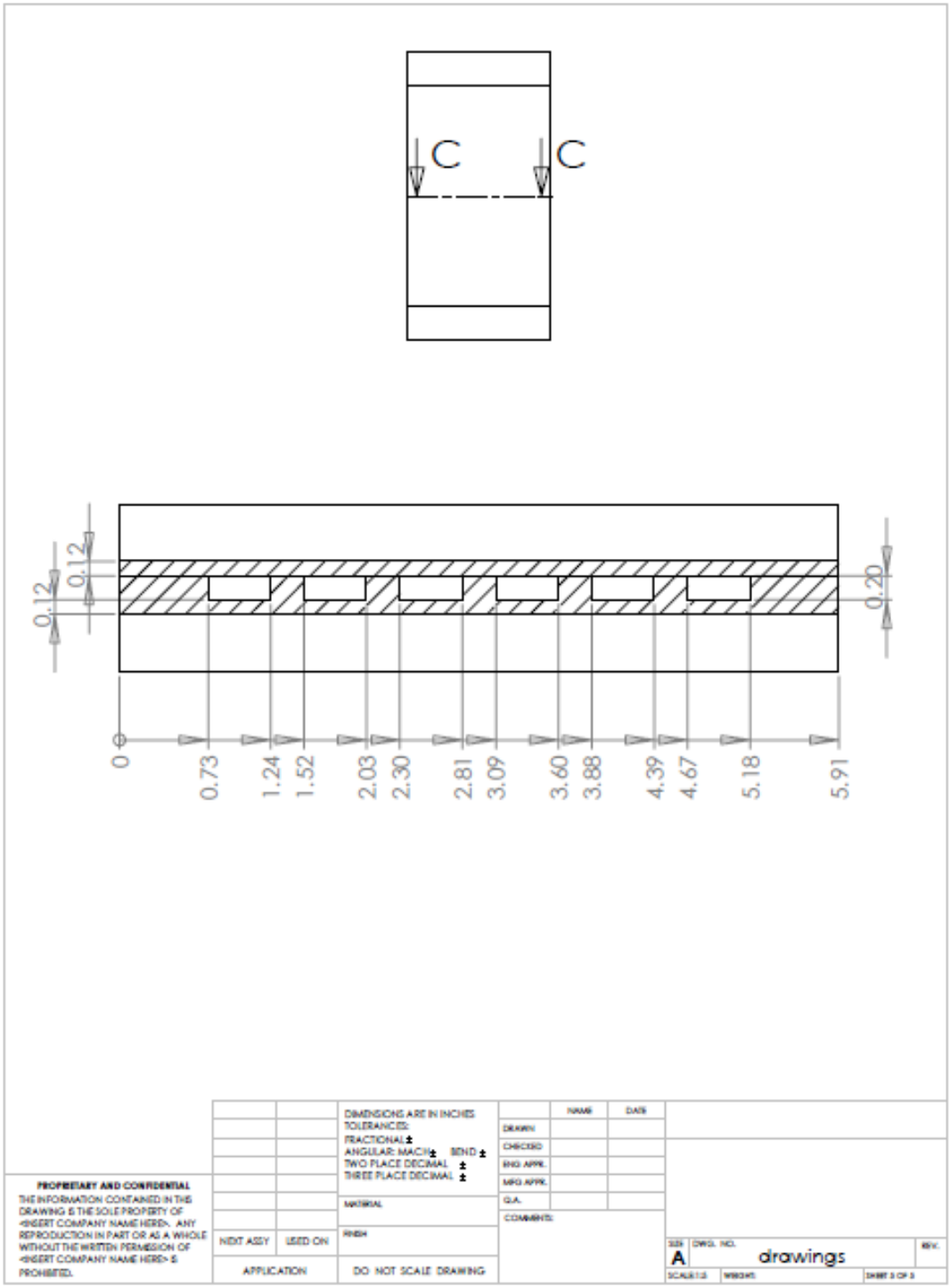

Condenser assembly:

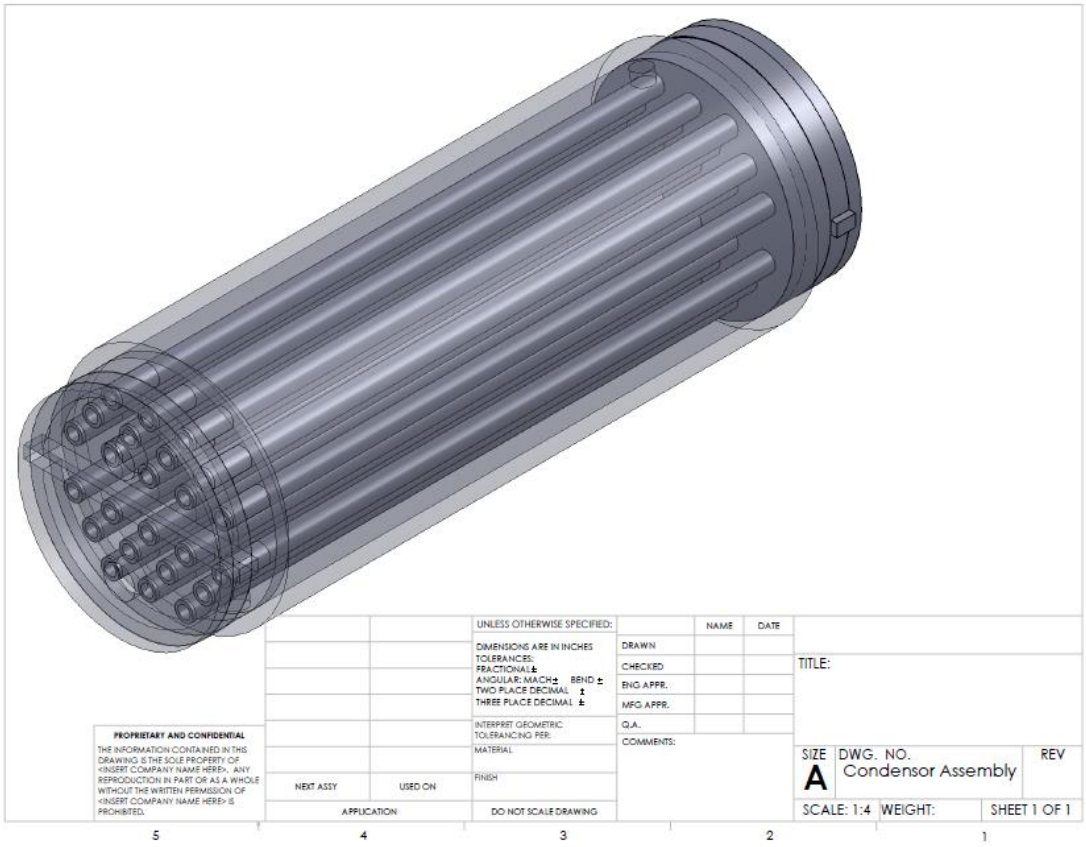

Condenser ends

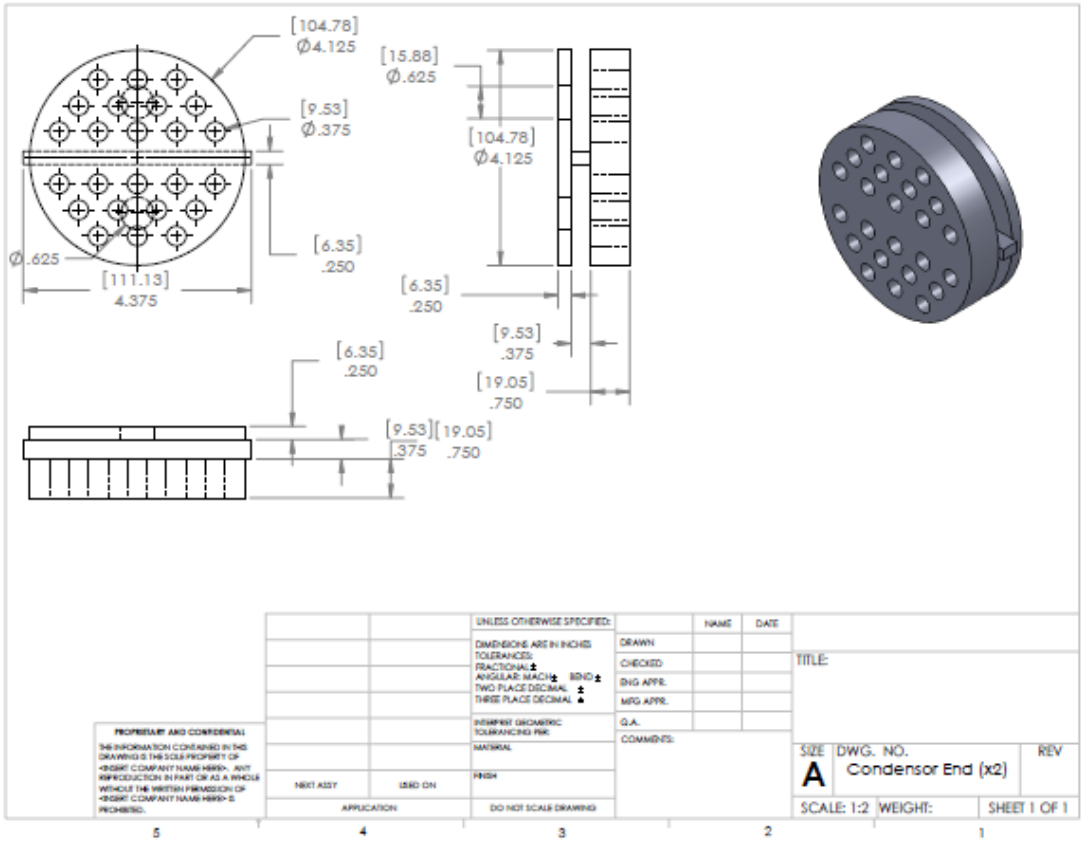
[104.78]
Ø4.125
[15.88]
Ø.625
[9.53]
Ø.375
[104.78]
Ø4.125
[6.35]
.250
Ø.625
[111.13]
4.375
[6.35]
.250
[9.53]
.375
[19.05]
.750
[6.35]
.250
[9.53]
.375
[19.05]
.750
UNLESS OTHERWISE SPECIFIED:
DIMENSIONS ARE IN INCHES
TOLERANCES:
FRACTIONAL ±
ANGULAR: MACH ± BEND ±
TWO PLACE DECIMAL ±
THREE PLACE DECIMAL ±
INTERPRET GEOMETRIC TOLERANCING PER:
MATERIAL
FINISH
DO NOT SCALE DRAWING
NAME
DATE
DRAWN
CHECKED
ENG APPR.
MFG APPR.
Q.A.
COMMENTS:
TITLE:
SIZE
A
DWG. NO.
Condensor End (x2)
REV
SCALE: 1:2
WEIGHT:
SHEET 1 OF 1
NEXT ASSY
USED ON
APPLICATION
PROPRIETARY AND CONFIDENTIAL
THE INFORMATION CONTAINED IN THIS DRAWING IS THE SOLE PROPERTY OF <INSERT COMPANY NAME HERE>. ANY REPRODUCTION IN PART OR AS A WHOLE WITHOUT THE WRITTEN PERMISSION OF <INSERT COMPANY NAME HERE> IS PROHIBITED.

Condenser chamber

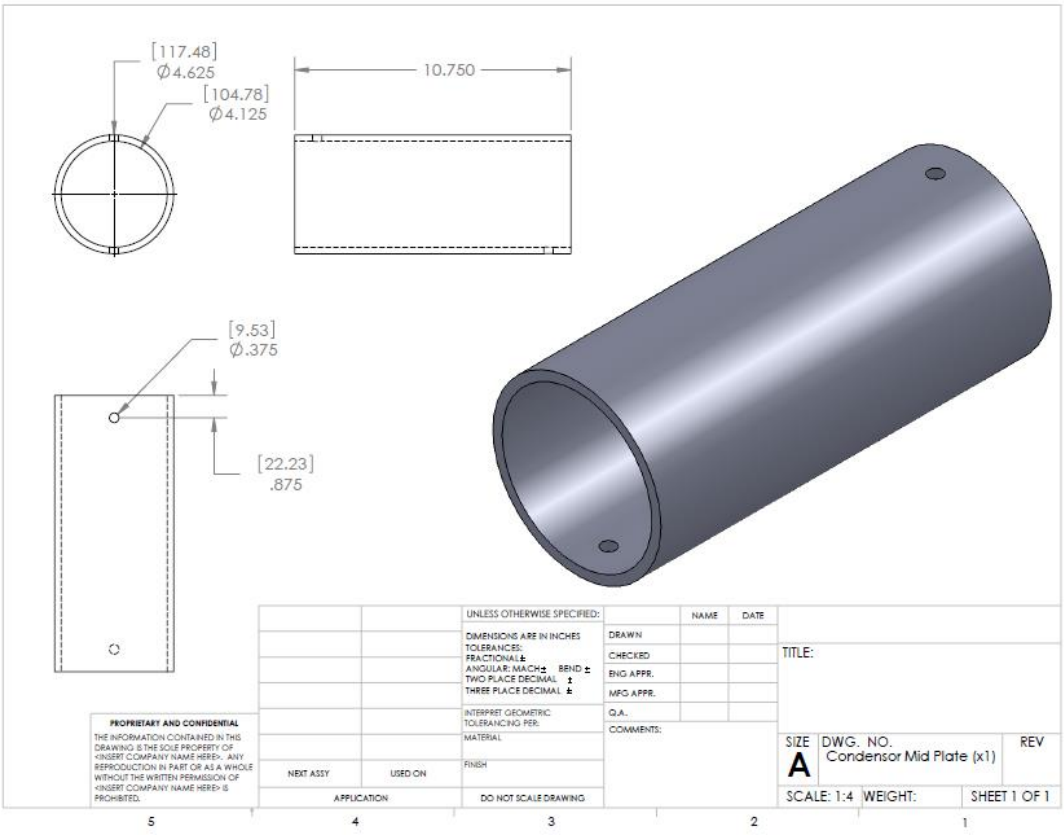

VITA

MAJID ALMAS

Born, Dhahran, Saudi Arabia

1998-2003	B.Sc., Marine Engineering Northumbria University Newcastle, UK
2003-2008	Vela International Marine, UAE
2008-2010	T.A. at King Abdul-Aziz University, Saudi Arabia
2011-2013	M.S., Mechanical Engineering Florida International University Miami, Florida
2014 -2020	Doctoral Candidate Florida International University Miami, Florida

PUBLICATIONS AND PRESENTATIONS

Soleimanikutanaei, S., Almas, M., Popoola, OT., Cao, Y. (2019). Reciprocating liquid-assisted system for electronic cooling applications. *Heat Transfer Asian Research*; 48, 286- 299.

Almas, M. (2016). Numerical modeling of turbulent flow inside the centrifugal blower. *Journal of Advances in Applied Computational Mathematics*, 3, 54-57.

Almas, M. (2014). Finite element simulation of jet combustor using local extinction approach with in eddy dissipation concept. *Journal of Advanced Thermal Science Research*, 1, 57-65.